The phytosphingosine degradation pathway includes fatty acid α-oxidation reactions in the endoplasmic reticulum

Takuya Kitamura[a], Naoya Seki[a], and Akio Kihara[a,1]

[a]Laboratory of Biochemistry, Faculty of Pharmaceutical Sciences, Hokkaido University, Kita 12-jo, Nishi 6-chome, Kita-ku, Sapporo 060-0812, Japan

[1]To whom correspondence should be addressed:

Akio Kihara

Laboratory of Biochemistry, Faculty of Pharmaceutical Sciences

Hokkaido University

Kita 12-jo, Nishi 6-chome, Kita-ku, Sapporo 060-0812, Japan

Tel: +81-11-706-3754

Fax: +81-11-706-4900

E-mail: kihara@pharm.hokudai.ac.jp

Abstract

Although normal fatty acids (FAs) are degraded via β-oxidation, unusual FAs such as 2-hydroxy (2-OH) FAs and 3-methyl-branched FAs are degraded via α-oxidation. Phytosphingosine (PHS) is one of the long-chain bases (the sphingolipid components) and exists in specific tissues, including the epidermis and small intestine in mammals. In the degradation pathway, PHS is converted to 2-OH palmitic acid and then to pentadecanoic acid (C15:0-COOH) via FA α-oxidation. However, the detailed reactions and genes involved in the α-oxidation reactions of the PHS degradation pathway have yet to be determined. In the present study, we reveal the entire PHS degradation pathway: PHS is converted to C15:0-COOH via six reactions [phosphorylation, cleavage, oxidation, CoA addition, cleavage (C1 removal), and oxidation], in which the last three reactions correspond to the α-oxidation. The aldehyde dehydrogenase ALDH3A2 catalyzes both the first and second oxidation reactions (fatty aldehydes to FAs). In *Aldh3a2*-deficient cells, the unmetabolized fatty aldehydes are reduced to fatty alcohols and are incorporated into ether-linked glycerolipids. We also identify HACL2 [previous name, ILVBL; ilvB (bacterial acetolactate synthase)-like] as the major 2-OH acyl-CoA lyase involved in the cleavage (C1 removal) reaction in the FA α-oxidation of the PHS degradation pathway. HACL2 is localized in the endoplasmic reticulum. Thus, in addition to the already-known FA α-oxidation in the peroxisomes, we have revealed the existence of FA α-oxidation in the endoplasmic reticulum in mammals.

Keywords: α-oxidation; fatty acid; metabolism; lipid; sphingolipid.

Significance statement

Although the synthetic pathway of phytosphingosine is already known, its degradation pathway has remained unclear. In the present study, we reveal the entire phytosphingosine degradation pathway, where fatty acid α-oxidation is involved. We show that the Sjögren-Larsson syndrome-causative gene *ALDH3A2* and *HACL2* are involved in the fatty acid α-oxidation reactions as an aldehyde dehydrogenase and a 2-hydroxy acyl-CoA lyase, respectively. Our findings are important for understanding the molecular mechanism of phytosphingosine/sphingolipid homeostasis. HACL2 is localized in the endoplasmic reticulum, indicating that fatty acid α-oxidation occurs in the endoplasmic reticulum in mammals, in addition to the α-oxidation already known to occur in peroxisomes.

Introduction

Most cellular fatty acids (FAs) have a non-hydroxylated straight chain and are degraded via β-oxidation either in the mitochondria for long-chain FAs (C11-C20), or in the peroxisomes for very long-chain FAs (≥C21) (1, 2). However, unusual FAs, such as 2-hydroxy (2-OH) FAs and 3-methyl-branched FAs (*i.e.*, food-derived phytanic acid), are degraded via α-oxidation (2-4). During FA synthesis by FA synthase type I, acetyl-acyl carrier proteins (ACPs) receive two-carbon units from malonyl-ACP seven times to produce palmitoyl-ACP, followed by thioester bond cleavage to release palmitic acid (C16:0-COOH) (5). Some of the cellular FAs are further elongated via the FA elongation cycle in the endoplasmic reticulum (ER). In each cycle, the FA chain-length is elongated by two (6, 7). In the FA degradation pathway (β-oxidation), the FA chain-length is shortened by two as acetyl-CoA is released (1). Thus, all FA synthesis, elongation, and degradation steps proceed by two-carbon units. Accordingly, most cellular FAs are even-numbered. However, odd-numbered FAs also exist, albeit at much lower levels, since α-oxidation produces odd-numbered FAs from 2-OH FAs (8, 9).

Sphingolipids are one of the major lipid classes in eukaryotes. The sphingolipid backbone ceramide (CER) is composed of a long-chain base (LCB) and an FA (10, 11). Although the FA moiety of CERs is non-hydroxylated in most tissues, CERs with 2-OH FA exist in specific tissues such as the epidermis and brain (11, 12). In accordance with the distribution pattern of 2-OH FA, the levels of odd-numbered CERs/sphingolipids are especially high in these tissues (13, 14). In the myelin of the brain, a high proportion of sphingolipids, especially galactosylceramide and its sulfated derivative sulfatide, contain a 2-OH FA (13, 15, 16). Their 2-OH groups are important for the formation and maintenance of the myelin sheath, which is composed of a multi-layered lipid structure, probably by

enhancing lipid-lipid interactions via hydrogen bonds. The FA 2-hydroxylase FA2H catalyzes conversion of FAs to 2-OH FAs (12, 17). Reflecting the importance of the 2-OH groups of galactosylceramide and sulfatide in myelin, *FA2H* mutations cause hereditary spastic paraplegia in human (18, 19) and late-onset axon and myelin sheath degeneration in mice (16, 20). To maintain the homeostasis of cellular 2-OH FAs, both the synthetic pathway and the degradation pathway (α-oxidation) are important. However, the details of the FA α-oxidation pathway remain unestablished.

Several types of LCBs exist in mammals; sphingosine (SPH), which contains a *trans* double bond between the C4-C5 positions (Fig. S1*A*), is the most abundant and exists ubiquitously. The saturated LCB dihydrosphingosine (DHS) also exists ubiquitously but at lower levels than SPH. We recently determined the entire degradation pathways of SPH and DHS (21-23) (Fig. S1*B*). These pathways convert LCBs to palmitoyl-CoA (C16:0-CoA) via four (for DHS) or five (for SPH) reactions. The generated C16:0-CoA is incorporated into several lipids, mainly into glycerolipids. These pathways are important for LCB homeostasis. Disruption of the SPH 1-phosphate lyase gene *Sgpl1*/*Spl*, which is responsible for the first, irreversible reaction of the LCB degradation pathways, causes several harmful effects in mice, including disturbance of lipid homeostasis in the liver, lesions in several tissues, and early death (around one month after birth) (24, 25).

Phytosphingosine (PHS) is another type of LCB in mammals and has an extra hydroxyl group at C4 (Fig. S2*A*). It exists in specific tissues such as the epidermis, small intestine, and kidney (11). Levels of PHS-containing CERs (PHS-CERs) are reduced in atopic dermatitis patients (26), implying the importance of PHS-CERs in epidermal permeability barrier formation. We recently revealed that PHS is metabolized to pentadecanoic acid (C15:0-COOH) via 2-OH C16:0-COOH in yeast and mammals (27). Thus, the PHS degradation

pathway is another supply source of 2-OH FAs, in addition to FA2H. Although the anterior half of the PHS degradation pathway is similar to those of DHS and SPH (Figs. S1 and S2), the latter half is completely different and largely unknown but includes an FA α-oxidation step (27). We identified *MPO1* as a gene involved in the PHS degradation pathway, likely in the FA α-oxidation step, in yeast (27), whereas a Mpo1 homolog does not exist in mammals. Thus, mammals must contain another type of FA α-oxidation enzyme(s).

In the present study, we determine the entire PHS degradation pathway and identify genes involved in the pathway in mammals. To date, only peroxisomal FA α-oxidation has been described in mammals (2, 28). The 2-OH acyl-CoA lyase HACL1, which is localized in the peroxisomes, has been shown to be involved in the cleavage (C1 removal) step of the FA α-oxidation that is composed of three reactions (CoA addition, cleavage, and oxidation) (3, 4, 29). Here, we show that the HACL1 homolog HACL2 [previous name, ILVBL; ilvB (bacterial acetolactate synthase)-like], which is localized in the ER, is mainly involved in the C1 removal reaction of the FA α-oxidation in the PHS degradation pathway. Thus, this is the first report describing the existence of FA α-oxidation in the ER in mammals.

Results

ALDH3A2 is Involved in the PHS Degradation Pathway. We previously revealed that PHS was metabolized to C15:0-COOH and mainly incorporated into ester-linked glycerolipids in mammalian cells (HEK 293T cells and mouse embryonic carcinoma F9 cells) (27) (Fig. S2*C*). The metabolism of PHS was dependent on SPH 1-phosphate lyase *Sgpl1* as other LCBs (27), indicating that PHS is first converted to PHS 1-phosphate by SPH kinase and then cleaved to 2-OH hexadecanal (2-OH C16:0-CHO) by SPH 1-phosphate lyase upstream of the PHS degradation pathway. However, detailed downstream reactions linking 2-OH C16:0-CHO to C15:0-COOH and the responsible genes remained unclear (Fig. S2*C*). By way of analogy to the degradation pathways of DHS and SPH (Figs. S1 and S2), we anticipated that 2-OH C16:0-CHO would be converted to 2-OH C16:0-COOH by the fatty aldehyde dehydrogenase (FALDH) ALDH3A2. *ALDH3A2* is the causative gene of the neurocutaneous disorder Sjögren-Larsson syndrome (30).

We examined the involvement of *ALDH3A2* in the PHS degradation pathway using an *Aldh3a2*-deficient derivative of CHO-K1 cells (FAA-K1A cells). The *Aldh3a2* deficiency causes a reduction in FALDH activity to ~10% of wild type CHO-K1 cells (31). We previously revealed that the metabolism of SPH and DHS to ester-linked glycerolipids was reduced in FAA-K1A cells and *Aldh3a2* knockout (KO) keratinocytes; instead, SPH and DHS were unusually metabolized to ether-linked glycerolipids, plasmanylethanolamine/plasmenylethanolamine (PlsE; plasmenylethanolamine, also known as ethanolamine plasmalogen) and plasmanylcholine (PlsC) (21, 32). In those cells, unmetabolized fatty aldehydes are reduced to fatty alcohols and then incorporated into ether-linked glycerolipids (Fig. S2*B*). Essentially the same results were obtained in the present study. When FAA-K1A cells were labeled with [^{3}H]DHS, the metabolism of DHS to ester-

linked glycerolipids was reduced, but metabolism to ether-linked glycerolipids was increased (Fig. 1*A*, lane 2). Alkaline treatment, which hydrolyzes ester-linkages, converted PlsE (lane 2, closed circle) to 1-alkyl/alkenyl-glycerophosphoethanolamine (A-GPE) and its undefined degradation products (A-GPE'; lane 6, open circles), which might be generated due to the reactive vinyl ether double bond of plasmenylethanolamine. PlsC (lane 2, closed square) was converted to 1-alkyl-glycerophosphocholine (A-GPC; lane 6, open square) by alkaline treatment.

[^{3}H]PHS was metabolized both to sphingolipids [CER, sphingomyelin (SM), glucosylceramide (GlcCER), etc.] via the sphingolipid biosynthetic pathway and to glycerolipids [phosphatidylethanolamine (PE), phosphatidylserine (PS), phosphatidylinositol (PI), and phosphatidylcholine (PC)] via the PHS degradation pathway (Fig.1*A* and Fig. S2*C*). Comparing sphingolipid metabolite levels of [^{3}H]PHS (Fig. 1*A*, lanes 3 and 7) with those of [^{3}H]DHS (lanes 1 and 5) in CHO-K1 cells, levels of SM labeled with [^{3}H]PHS (*i.e.*, PHS-SM) were slightly lower than those of SM labeled with [^{3}H]DHS (*i.e.*, mixture of DHS-SM and SPH-SM; Fig. S2*B*). On the other hand, levels of GlcCER labeled with [^{3}H]PHS (*i.e.*, PHS-GlcCER) were higher than those of GlcCER labeled with [^{3}H]DHS (*i.e.*, a mixture of DHS-GlcCER and SPH-GlcCER). These results suggest that GlcCER synthase (UDP-glucose ceramide glucosyltransferase) prefers PHS-CER as a substrate than CER but SM synthase does not. Furthermore, 2-OH PHS-GlcCER (PHS-GlcCER having a 2-OH FA) was detected in the [^{3}H]PHS labeling (Fig. 1*A*, lanes 3 and 7), indicating that PHS is not only incorporated into PHS-GlcCER as an LCB but is also incorporated as a 2-OH FA, which is generated via the PHS degradation pathway (Fig. S2*C*). In FAA-K1A cells, PHS was not metabolized to 2-OH PHS-GlcCER (Fig. 1*A*, lanes 4 and 8), indicating that ALDH3A2 is

involved in the conversion of 2-OH C16:0-CHO to 2-OH C16:0-COOH in the PHS degradation pathway as expected.

Conversion of [^{3}H]PHS to ester-linked glycerolipids in the PHS degradation pathway was impaired in FAA-K1A cells similar to the cases of [^{3}H]DHS and [^{3}H]SPH (21) (Fig. 1*A*, lanes 4 and 8). Levels of PC labeled with [^{3}H]PHS and those of released FAs by alkaline treatment were lower in FAA-K1A cells (lanes 4 and 8) than those in CHO-K1 cells (lanes 3 and 7). On the other hand, levels of ether-linked ethanolamine glycerolipids (2-OH PlsE) were increased (lanes 4 and 8).

We next examined the conversion of PHS to 2-OH CER by liquid chromatography (LC)-tandem mass spectrometry (MS/MS) analysis. Although PHS-CER was absent both in CHO-K1 and FAA-K1A cells under normal growth conditions, the addition of PHS to the medium resulted in production of PHS-CER (Fig. 1*B*). PHS addition also caused increases in the levels of 2-OH CER and 2-OH PHS-CER in CHO-K1 cells. However, such increases were not observed in FAA-K1A cells. This result was consistent with the above data obtained from the [^{3}H]PHS labeling experiment (Fig. 1*A*), in which 2-OH PHS-GlcCER production was dependent on the presence of intact *Aldh3a2*. In conclusion, PHS is mainly converted to C15:0-COOH and incorporated into ester-linked glycerolipids in the degradation pathway under normal (*Aldh3a2*-active) conditions, whereas some fraction of PHS is also converted to the 2-OH FA moiety of sphingolipids. In addition, our results indicate that ALDH3A2 is involved in the PHS degradation pathway by converting 2-OH C16:0-CHO to 2-OH C16:0-COOH.

HACL2 is a 2-OH Acyl-CoA Lyase Involved in the PHS Degradation Pathway. PHS is a major LCB in yeast. We previously identified yeast *MPO1* as the gene involved in the PHS

degradation pathway, maybe at the α-oxidation step (27). Although Mpo1 is conserved in bacteria, fungi, plants, and protists, its homolog does not exist in mammals. On the other hand, peroxisome-localized 2-OH acyl-CoA lyase HACL1 has been suggested to be involved in the C1 removal step in the α-oxidation reactions of 2-OH FA metabolism in mammals from *in vitro* experiments (3). However, it has not yet been determined whether HACL1 indeed functions in FA α-oxidation within cells. HACL2/ILVBL is a homolog of HACL1 (22.5% identity and 42.0% similarity). The function or activity of HACL2 has not yet been determined. We examined the involvement of HACL1 and HACL2 in the PHS degradation pathway using *MPO1*-deleted yeast cells (*mpo1*Δ). Consistent with our previous report (27), *mpo1*Δ cells bearing the empty vector could not convert [^{3}H]PHS to glycerolipids (PE, PC, PS, and PI), although they could convert it to complex sphingolipids [inositol phosphorylceramide (IPC), mannosylinositol phosphorylceramide (MIPC), and mannosyldiinositol phosphorylceramide (M(IP)$_2$C)] (Fig. 2*A*). Expression of 3xFLAG-tagged Mpo1 in *mpo1*Δ cells recovered the metabolism of PHS to glycerolipids. Ectopic expression of 3xFLAG-tagged HACL1 weakly rescued the deficient PHS-to-glycerolipid conversion. 3xFLAG-tagged HACL2 also rescued the conversion, and to a greater degree than HACL1. The protein expression levels of 3xFLAG-tagged HACL2 in the yeast were lower than those of 3xFLAG-tagged HACL1 (Fig. 2*B*), suggesting that the activity of HACL2 was higher than that of HACL1.

HACL1 catalyzes the conversion of 2-OH hydroxy acyl-CoA (n) to fatty aldehyde (n-1) in a thiamine pyrophosphate (TPP)-dependent manner (3). We examined substrate and product of HACL2 using affinity-purified 3xFLAG-tagged HACL2 *in vitro*. Consistent with the previous report (3), 3xFLAG-tagged HACL1 produced fatty aldehyde from 2-OH C18:0-CoA (Fig. 2*C*). Similarly, 3xFLAG-tagged HACL2 generated fatty aldehyde from 2-OH

C18:0-CoA but not from 2-OH C18:0-COOH. The reaction by HACL2 was TPP-dependent, similar to that of HACL1 (Fig. 2*D*). These results indicate that HACL2 is also a TPP-dependent 2-OH acyl-CoA lyase. Although HACL2 has been known as ILVBL [ilvB (bacterial acetolactate synthase)-like], we renamed it HACL2 to represent its function in the present study.

Involvement of HACL1 and HACL2 in the PHS degradation pathway was examined using mammalian cells (CHO-K1 cells). Real-time quantitative RT-PCR analysis revealed that levels of *Hacl1* mRNA were >10-fold higher than those of *Hacl2* mRNA in CHO-K1 cells (Fig. 3*A*). We created *Hacl1* and *Hacl2* single gene KO cells, as well as *Hacl1 Hacl2* double KO (DKO) CHO-K1 cells using the CRISPR-Cas9 system (Fig. S3). Metabolism of [^{3}H]DHS was similar among control, *Hacl1* KO, *Hacl2* KO, and *Hacl1 Hacl2* DKO cells (Fig. S4). Disruption of *Hacl1* had no effect on [^{3}H]PHS metabolism (Fig. 3*B*). On the other hand, *Hacl2* KO cells exhibited altered metabolism of [^{3}H]PHS, with a reduced conversion to PC and an increased conversion to 2-OH PHS-GlcCER. *Hacl1 Hacl2* DKO cells showed more prominent effects on these metabolic changes. These results indicate that HACL1 and HACL2 possess redundant functions in the PHS degradation pathway, although the contribution of HACL2 is higher than HACL1. It is highly likely that the accumulated 2-OH C16:0-CoA (as the result of the impaired conversion of PHS-derived 2-OH C16:0-CoA to C15:0-CHO) was used as an acyl-CoA donor for CER synthase, leading to an increase in 2-OH PHS-GlcCer levels in *Hacl2* KO and *Hacl1 Hacl2* DKO cells (Fig. S5).

We next examined the effect of *Hacl1* and/or *Hacl2* disruption on 2-OH C16:0-COOH metabolism by measuring odd-numbered PCs using LC-MS/MS analysis. The addition of 2-OH C16:0-COOH to the culture medium resulted in an increase in odd-numbered (C15:0 and C17:0) PCs in control cells, *Hacl1* KO cells, and *Hacl2* KO cells (Fig. 3*C* and Fig. S6*A*).

Some C15:0-CoA seemed to be elongated to C17:0-CoA before incorporating into PC. However, such an increase was not observed in *Hacl1 Hacl2* DKO cells. This result indicates the redundant functions of HACL1 and HACL2 in 2-OH C16:0-COOH metabolism. In this case, a higher contribution of HACL2 than HACL1 to the PHS degradation pathway revealed by the [^{3}H]PHS labeling experiment (Fig. 3*B*) was not observed. PHS addition had no effect on even-numbered PCs in any of the cells (Fig. 3*D* and Fig. S6*B*).

HACL2 is Localized in the ER. To examine the subcellular localization of the HACL2 protein, we performed indirect immunofluorescence microscopy. Consistent with the previous report that HACL1 is a peroxisome protein (29), 3xFLAG-tagged HACL1 exhibited a scattered, typical peroxisomal staining pattern (Fig. 4*A*). On the other hand, 3xFLAG-tagged HACL2 showed a reticular structure. The signal merged with an ER marker but not with a mitochondrial marker, indicating that HACL2 is an ER protein. Thus, the localizations of HACL1 and HACL2 differ.

When the total cell lysates of cells expressing 3xFLAG-tagged HACL1 or HACL2 were fractionated into soluble and membrane fractions by ultracentrifugation, HACL1 was detected in the soluble fraction (Fig. 3*B*). On the other hand, HACL2 was recovered in the membrane fraction. These results indicate that HACL1 is localized in the lumen of peroxisomes, while HACL2 is an ER membrane protein. HACL2 contains a highly hydrophobic stretch at the N-terminus, which may act as a transmembrane segment.

We next investigated the tissue specific expression patterns of *HACL1* and *HACL2* mRNAs using quantitative real-time RT-PCR. Both *HACL1* and *HACL2* were expressed ubiquitously (Fig. 4*C*). In many tissues/cells such as pancreas, colon, kidney, heart, spleen,

thymus, ovary, prostate, and differentiated keratinocytes, expression levels of *HACL2* were higher than those of *HACL1*.

ALDH3A2 is Responsible for Two Oxidation Reactions in the PHS Degradation Pathway. The HACL product C15:0-CHO must be converted to C15:0-COOH before being incorporated into glycerolipids (Fig. S5). Aldehyde-to-carboxylic acid conversion reactions are catalyzed by aldehyde dehydrogenases (ALDHs). Among ~20 ALDHs in mammals (19 in human and 21 in mouse), ALDH3 subfamily members (ALDH3A1, A2, and B1 in human) are responsible for the oxidation of long-chain aldehydes (33, 34). Among the ALDH3 subfamily members, only ALDH3A2 is localized to the ER (35), the same site as HACL2, whereas the minor splicing isoform of ALDH3A2 is localized to the peroxisomes (35). As described above, ALDH3A2 is involved in the oxidation step (conversion of 2-OH C16:0-CHO to 2-OH C16:0-COOH) upstream of the HACL-mediated α-oxidation reaction (Fig. 1 and Fig. S5). We examined the possibility that ALDH3A2 is also involved in another oxidation step (conversion of C15:0-CHO to C15:0-COOH) downstream of the HACL-mediated C1 removal reaction by [^{3}H]2-OH C16:0-COOH labeling. Metabolism of non-hydroxy [^{3}H]C16:0-COOH (palmitic acid) was similar between CHO-K1 and *Aldh3a2*-deficient FAA-K1A cells (Fig. 5*A*). On the other hand, metabolism of [^{3}H]2-OH C16:0-COOH was altered in FAA-K1A cells: metabolism of [^{3}H]2-OH C16:0-COOH to glycerolipids was reduced in FAA-K1A cells compared to CHO-K1 cells; instead, metabolism to ether-linked glycerolipids was increased. This result suggests that unmetabolized C15:0-CHO was reduced to pentadecanol (C15:0-OH) and used for ether-linked glycerolipid synthesis. Add-back of *ALDH3A2* into FAA-K1A cells (FAA-ALDH3A2

cells; FAA-K1A cells stably expressing *3xFLAG-ALDH3A2*) recovered the impaired [^{3}H]2-OH C16:0-COOH metabolism.

We confirmed the above result by LC-MS/MS analysis. The addition of 2-OH C16:0-COOH to the culture medium resulted in an increase in the levels of odd-numbered PCs (Fig. 5*B* and Fig. S7*A*). However, such an increase was not observed in FAA-K1A cells. Again, the introduction of *ALDH3A2* into FAA-K1A cells recovered the increase. Levels of even-numbered PCs were almost not affected by the addition of 2-OH C16:0-COOH or by *Aldh3a2* disruption (Fig. 5*C* and Fig. S7*B*). These results indicate that ALDH3A2 is involved in both the first and second oxidation steps in the PHS degradation pathway.

Discussion

In general, the levels of biomolecules are kept within a narrow range as a result of an appropriate balance between synthesis and degradation. If such homeostasis is impaired, certain cell functions might be damaged, possibly leading to disorders. Since 2-OH FAs are exclusively used for sphingolipid synthesis but not for the synthesis of other lipids such as glycerolipids, 2-OH FAs must be converted to metabolizable compounds, *i.e.*, non-hydroxy, odd-numbered FAs. Non-hydroxy FAs, regardless of whether they are even-numbered or odd-numbered, can be metabolized to several lipids (27). Thus, FA α-oxidation should be important for 2-OH FA homeostasis, but not for the production of odd-numbered FAs. To date, only the peroxisome is known to be the site of FA α-oxidation in mammals. However, HACL2 is localized in the ER (Fig. 4*A*), indicating that FA α-oxidation also occurs there. The existence of FA α-oxidation in the ER is quite reasonable, since PHS degradation takes place in the ER (see below).

Here, we revealed the missing link from 2-OH C16:0-CHO to C15:0-COOH in the PHS degradation pathway (Fig. 6), leading to understanding of the entire PHS degradation pathway. PHS is first phosphorylated to PHS 1-phosphate by SPH kinase. Mammals have two SPH kinases: SPHK1 and SPHK2. SPHK2 can phosphorylate all three types of LCBs (DHS, SPH, and PHS), whereas the activity of SPHK1 toward PHS is quite low (36, 37). Thus, SPHK2 is mainly involved in the synthesis of PHS 1-phosphate. There are two steps converting FAs to acyl-CoAs (conversion of 2-OH C16:0-COOH to 2-OH C16:0-CoA and conversion of C15:0-COOH to C15:0-CoA) in the PHS degradation pathway. Acyl-CoA synthetases (ACSs) are responsible for these conversions. Humans have 26 ACSs, which are classified into six subfamilies (ACSS, ACSM, ACSL, ACSVL, ACSF, and ACSBG) depending on their substrate specificities toward acyl-CoA chain-lengths and sequence

similarity (38). Of the ACS subfamilies, the ACSL subfamily, consisted of ACSL1, 3, 4, 5, and 6, is mainly responsible for the conversion of long-chain FAs to acyl-CoAs (39). We previously revealed that ACSL1, 3, 4, 5, 6, VL1, 4, and BG1 are involved in the DHS and SPH degradation pathways (21, 22). It is likely that these ACSs are also involved in the PHS degradation pathway.

Although HACL1 and HACL2 are redundantly involved in the C1 removal step in the PHS degradation pathway, HACL2 provides the main function in this pathway. In the [^{3}H]PHS labeling experiment, disruption of *Hacl2* caused altered [^{3}H]PHS metabolism: decreased metabolism to PC and increased metabolism to 2-OH PHS-GlcCER (Fig. 3*B*). On the other hand, *Hacl1* disruption had no effect. We speculate that the differences in the localization of HACL1 (peroxisome) and HACL2 (ER) determines the degree of their contribution to the PHS degradation pathway. All the enzymes acting downstream of PHS 1-phosphate, *i.e.* SGPL1, ALDH3A2, and ACSLs, are all localized in the ER (22, 35, 40): in other word, PHS degradation occurs in the ER. In *Hacl2*-deficient cells, unmetabolized 2-OH C16:0-CoA in the ER may be unusually delivered to peroxisomes and is subjected to the C1 removal reaction by HACL1.

In contrast to the higher contribution of HACL2 than HACL1 to the PHS degradation pathway, HACL1 and HACL2 seem to contribute similarly to the metabolism of exogenously added 2-OH C16:0-COOH (Fig. 3*C*). As described above, 2-OH C16:0-CoA is generated in the ER from PHS. Therefore, the ER-localized HACL2 mainly acts on PHS-derived 2-OH C16:0-CoA. On the other hand, it is likely that exogenously added 2-OH C16:0-COOH is converted to 2-OH C16:0-CoA by plasma membrane-localized ACSs and is moved to both the ER and peroxisomes for further metabolism. Thus, the different sites of 2-OH C16:0-CoA production may cause the different HACL contributions to its metabolism. Our results were

consistent with the previous report. When exogenously added 2-OH C18:0-COOH metabolism was examined using cells defective in peroxisomal protein targeting (Zellweger fibroblasts and *Pex5*-null fibroblasts), removal of the C1 carbon was reduced to approximately half in the mutant fibroblasts compared to control fibroblasts (3). This result also suggests that the contributions of peroxisomal HACL1 and other 2-OH acyl-CoA lyase localized outside peroxisomes (maybe ER-localized HACL2 considering our results) to metabolism of exogenously added 2-OH C18:0-COOH are similar.

ALDH3A2 is the causative gene of the neurocutaneous disorder Sjögren-Larsson syndrome (30). Since aldehyde molecules are reactive and thus generally toxic, accumulated fatty aldehydes in the Sjögren-Larsson syndrome patients are considered to be responsible for pathogenesis. For this reason, generated aldehydes must be removed rapidly. Thus, the coincidence of the both the C15:0-CHO–generating (HACL2) and C15:0-CHO–removing (ALDH3A2) enzymes in the ER seems to be important to prevent cell toxicity.

The PHS degradation pathway is not a sole supply source of 2-OH FAs. The FA 2-hydroxylase FA2H directly forms 2-OH FAs from FAs (12, 17). Although the PHS degradation pathway generates 2-OH C16:0-COOH almost exclusively, FA2H can produces 2-OH FAs ranging from long-chain to very long-chain (17, 41). 2-OH very long-chain FAs with C22 or C24 chain-length exist abundantly in galactosylceramides and sulfatides in myelin and are important for myelin function and maintenance (16, 18-20). Very long-chain FAs are degraded in peroxisomes. Therefore, it is possible that HACL1 is mainly responsible for the α-oxidation of 2-OH very long-chain FAs, while HACL2 functions in the α-oxidation of 2-OH long-chain FAs; a possibility which must be tested in future studies.

In the present study, we found that some of the 2-OH C16:0-CoAs derived from PHS were used for the 2-OH FA moiety of 2-OH sphingolipids (2-OH PHS-CER and 2-OH PHS

GlcCER; Fig. 1). In *Hacl2* KO and *Hacl1 Hacl2* DKO cells, 2-OH PHS-GlcCER levels were further increased (Fig. 3*B*). Thus, 2-OH FAs in 2-OH sphingolipids are supplied not only from FA2H but also from the PHS degradation pathway (Fig. 6).

PHS derivatives (PHS containing a *cis* or *trans* double bond between C8 and C9) are abundant in plants (42). Although humans consume them in food, their metabolism is unclear. It is possible that they are converted to odd-numbered monounsaturated FAs via α-oxidation in a similar way as revealed here for PHS.

In conclusion, we identified FA α-oxidation reactions in the ER, which are involved in PHS degradation and maybe in the metabolism of 2-OH FA derived from other sources, such as the FA2H-mediated direct production from FAs. In addition, our results lead to the elucidation of the entire PHS degradation pathway. Further studies are needed to elucidate the physiological and pathological roles of α-oxidation of 2-OH FAs using *Hacl1* and *Hacl2* KO mice and *Hacl1 Hacl2* DKO mice.

Materials and Methods

Cell Culture and Transfection. CHO-K1, FAA-K1A (*Aldh3a2*-deficient derivative of CHO-K1 cells) (31), and FAA-ALDH3A2 (*3xFLAG-ALDH3A2* stable transformant of FAA-K1A cells) (21) cells were grown in Ham's F-12 medium (Sigma, St. Louis, MO) and HEK 293T cells and HeLa cells in Dulbecco's modified Eagle's medium (Sigma); each medium contained 10% fetal bovine serum, 100 units/ml penicillin, and 100 μg/ml streptomycin. HEK 293T cells were grown in dishes coated with 0.3% collagen. Human primary keratinocytes (CELLnTECH, Bern, Switzerland) were cultured in CnT prime Epidermal Keratinocyte Medium (CELLnTECH), and differentiation was induced by incubating the cells with CnT-Prime 3D Barrier Medium (CELLnTECH). Transfections were performed using Lipofectamine Plus™ Reagent (Thermo Fisher Scientific, Waltham, MA), according to the manufacturer's instructions.

Yeast Strains and Media. The *Saccharomyces cerevisiae* strain 4378 (*MAT**a** his3Δ1 leu2Δ0 met15Δ0 ura3Δ0 Δmpo1::KanMX4*) was described previously (27, 43). Cells were grown in synthetic complete medium lacking uracil (0.67% yeast nitrogen base, 2% D-glucose, 0.5% casamino acids, 20 mg/l adenine, and 20 mg/l tryptophan) at 30 °C.

Plasmids. The pCE-puro 3xFLAG-1 (mammalian vector; for N-terminal 3xFLAG tag) (44), pCE-puro 3xFLAG-4 (mammalian vector; for C-terminal 3xFLAG tag) (45), and pAKNF316 (yeast vector; for N-terminal 3xFLAG tag; *URA3* marker) (21) plasmids are mammalian or yeast expression vectors under the control of human elongation factor 1α or yeast glyceraldehyde 3-phosphate dehydrogenase (GAPDH) promoter. Human *HACL1* and *HACL2* genes were amplified by PCR using the respective forward (-F) and reverse (-R) primers

(HACL1-F, 5'-GGATCCATGCCGGACAGTAACTTCGCAGAGC-3', *Bam*HI site underlined; HACL1-R, 5'-TTACATATTAGAGCGGGTCAGCCAA-3'; HCAL2-F1, 5'-GGATCCATGGAGACCCCCGCGGCCGCCGCCC-3', *Bam*HI site underlined; HACL2-R1, 5'-TGCGCACTATACAGCAATGGAGCCATCGCGG-3', *Fsp*I site underlined; HACL2-F2, 5'-GGATCCGCCACCATGGAGACCCCCGCGGCCGCCGCCC-3', *Bam*HI site underlined; and HACL2-R2, 5'-GGATCCACAGCAATGGAGCCATCGCGGAAGT-3') from human liver cDNA (Human MTC panel I; TAKARA Bio, Shiga, Japan). The amplified fragments were first cloned into the TA cloning vector pGEM-T Easy (Promega, Madison, WI), generating the pGEM-HACL1 (HACL1-F/R primers), pGEM-HACL2-N (HACL2-F1/R1 primers), and pGEM-HACL2-C (HACL2-F2/R2 primers) plasmids. Each gene was digested with appropriate restriction enzymes and transferred to pAKNF316, pCE-puro 3xFLAG-1, or pCE-puro 3xFLAG-4 vector. The generated plasmids were pTK183 (*HACL1*; transferred from pGEM-HACL1 to pAKNF316), pZKN14 (*HACL2*; transferred from pGEM-HACL2-N to pAKNF316), pCE-puro 3xFLAG-HACL1 (*HACL1*; transferred from pGEM-HACL1 to pCE-puro 3xFLAG-1), and pCE-puro HACL2-3xFLAG (*HACL2*; transferred from pGEM-HACL2-C to pCE-puro 3xFLAG-4) plasmids. The *MPO1* gene was amplified from yeast genomic DNA using the primers (MPO1-F, 5'-GGATCCATGGGCGAAGGTTTGCTGGATTTAAG-3', *Bam*HI site underlined; and MPO1-R, 5'-TTATTGTCTTTGCATCCGCAAATTTC-3'). The amplified fragment was cloned into the pGEM-T Easy vector, digested with *Bam*HI and *Not*I, and transferred to the pAKNF316 vector, generating the pNK46 (*3xFLAG-MPO1*) plasmid.

The all-in-one CRISPR/Cas9 vectors pX330Ab-puro-1x2 and pX330Sb-puro-2 are the derivatives of pX330A-1x2 and pX330S-2 (Multiplex CRISPR/Cas9 Assembly Systems Kit; Addgene, Cambridge, MA). The puromycin resistance gene was first inserted into the *Not*I

site of the pX330A-1x2 and pX330S-2 plasmids. The *Bbs*I sites of the resulting plasmids were then converted to *Bae*I sites, generating the pX330Ab-puro-1x2 and pX330Sb-puro-2 plasmids. Primers used to guide RNA expression were as follows: for *Hacl1* KO, primers Hacl1 KO-F1 (5'-CAAGGGCGATTTCGGTCACGGTTTT-3') and Hacl1 KO-R1 (5'-CGTGACCGAAATCGCCCTTGCGGTG-3'); for *Hacl2* KO, primers Hacl2 KO-F1 (5'-TTGCCATGCCACTCAAGGCGGTTTT-3') and Hacl2 KO-R1 (5'-CGCCTTGAGTGGCATGGCAACGGTG-3'); and for *Hacl1 Hacl2* DKO, primers Hacl1 KO-F2 (5'-TGAAGACAAAGCGTACACCAGTTTT-3'), Hacl1 KO-R2 (5'-TGGTGTACGCTTTGTCTTCACGGTG-3'), Hacl2 KO-F1, and Hacl2 KO-R1. Each forward primer was annealed with the respective reverse primer and inserted into the *Bae*I site of the pX330Ab-puro-1x2 or pX330Sb-puro-2 vector, generating the pX330Ab-puro-Hacl1-1, pX330Ab-puro-Hacl1-2, and pX330Sb-puro-Hacl2-1 plasmids. The pX330Ab-puro-Hacl1/2 plasmid was constructed by cloning the *Bsa*I fragment of the pX330Sb-puro-Hacl2-1 into the *Bsa*I site of the pX330Ab-puro-Hacl1-2 plasmid.

Construction of *Hacl* KO Cells. To obtain *Hacl1* KO, *Hacl2* KO, and *Hacl1 Hacl2* DKO cells, CHO-K1 cells were transfected with the all-in-one CRISPR/Cas9 plasmid (pX330Ab-puro-1x2 vector for control, pX330Ab-puro-Hacl1-1 for *Hacl1* KO, pX330Sb-puro-Hacl2-1 for *Hacl2* KO, or pX330Ab-puro-Hacl1/2 for *Hacl1 Hacl2* DKO). The transfected cells were subjected to selection in 10 μg/ml puromycin for two days. The medium was then changed to one without puromycin, and cells were cultured for a further five days. Several colonies were picked up, and clones with mutations in *Hacl1* and/or *Hacl2* loci (Fig. S3) were used for further analyses.

Membrane Fractionation. Cells were suspended in buffer A [50 mM HEPES-NaOH (pH 7.4), 150 mM NaCl, 10% glycerol, and 1mM dithiothreitol] containing 1x protease inhibitor mixture (Complete EDTA-free; Roche Diagnostics, Indianapolis, IN) and 1 mM phenylmethylsulfonyl fluoride. Cells were lysed by sonication, and cell debris was removed by centrifugation at 1,200 g, for 3 min at 4 °C. The resulting total lysates were centrifuged at 100,000 g for 30 min at 4 °C into pellet (membrane fraction) and supernatant (soluble fraction). The pellet was suspended in buffer A containing 1x protease inhibitor mixture and 1 mM phenylmethylsulfonyl fluoride by sonication.

Affinity-purification of 3xFLAG-tagged HACL1 and HACL2. 3xFLAG-HACL1 and HACL2-3xFLAG were affinity-purified using anti-FLAG M2 affinity agarose gel (Sigma), essentially as described previously (34). HEK 293T cells were transfected with pCE-puro 3xFLAG-HACL1 or pCE-puro HACL2-3xFLAG plasmid. Twenty-four hours after transfection, cells were subjected to membrane fractionation as described above. To purify 3xFLAG-HACL1, the supernatant (soluble fraction) was incubated with anti-FLAG M2 affinity agarose gel (Sigma) overnight at 4 °C with rotation. On the other hand, the pellet (membrane fraction) was used for HACL2-3xFLAG purification. The pellet was suspended in buffer A containing 1x protease inhibitor mixture, 1 mM phenylmethylsulfonyl fluoride, and 1.2% Triton-X 100 by sonication and was rotated at 4 °C for 30 min to facilitate solubilization. After centrifugation at 100,000 g for 30 min at 4 °C, the supernatant (solubilized fraction) was recovered and incubated with anti-FLAG M2 affinity agarose gel overnight at 4°C with rotation. Beads were washed three times with buffer A containing 0.1% Triton X-100, and bound proteins were eluted with buffer A containing 100 μg/ml 3xFLAG peptide and 0.1% Triton X-100.

***In Vitro* 2-OH Acyl-CoA Lyase Assay.** *In vitro* 2-OH acyl-CoA lyase assays were performed by incubating the affinity-purified HACL protein (1 μg) with 100 μM 2-OH C18-COOH (Matreya, State College, PA) or 2-OH C18:0-CoA (Avanti Polar Lipids, Alabaster, AL) in 100 μl of buffer A containing 1x protease inhibitor mixture, 0.1% TrintonX-100, 0.8 mM $MgCl_2$, and 20 μM TPP at 37 °C for 4 h. After reaction, lipids were extracted by successive addition and mixing of 375 μl of chloroform/methanol (1/2, v/v), 125 μl of chloroform, and 125 μl of water. The organic-phase was recovered by centrifugation, dried, and suspended in 20 μl of chloroform/methanol (2/1, v/v). Lipids were separated by TLC on Silica Gel 60 high performance TLC plates (Merck, Darmstadt, Germany) with hexane/diethyl ether/acetic acid (65/35/1, v/v) and stained by Schiff reagent (Wako Pure Chemical Industries, Osaka, Japan).

Lipid Labeling Assay. Lipid labeling assay was performed as described previously (21, 27). In some cases, the contrast of the images was enhanced through linear adjustment using Photoshop CS6 software (Adobe, San Jose, CA). [4, 5-^{3}H]DHS (60 Ci/mmol, 1 mCi/ml) and [9, 10-^{3}H]C16:0-COOH (60 Ci/mmol, 10 mCi/ml) were purchased from American Radiolabelling Chemicals (St. Louis, MO). [11, 12-^{3}H]PHS (0.1 mCi/ml, 0.4 mM) was prepared as described previously (27), whereas [9, 10-^{3}H]2-OH C16:0-COOH (0.03 mCi/ml, 0.12 mM) was prepared from [11, 12-^{3}H]PHS as follows. Membrane fractions were prepared from yeast strain 4378 (Δ*mpo1*) overproducing the 3xFLAG-tagged LCB kinase Lcb4 from the pZKN30 plasmid, and the HA-tagged LCB 1-phosphate lyase Dpl1 from the pAN18 plasmid, as described previously (46). [11, 12-^{3}H]PHS was converted to [9, 10-^{3}H]2-OH C16:0-COOH by incubating [11, 12-^{3}H]PHS with the prepared membrane fractions in buffer

A containing 1x protease inhibitor mixture, 1 mM phenylmethylsulfonyl fluoride, 1 mg/ml FA-free bovine serum albumin (Sigma), 5 mM $MgCl_2$, 4.5 mM ATP, 0.625 mM NAD^+, and 7.5 μM pyridoxal 5'-phosphate at 37 °C for 6 h. Lipids were then extracted as described above, dried, and suspended in ethanol. The converting efficiency from [11, 12-^{3}H]PHS to [9, 10-^{3}H]2-OH C16:0-COOH was nearly 100%.

Lipid Analysis by LC-MS/MS. Lipid extraction from cells was performed as described above. During extraction, C12:0/12:0 PC (Avanti Polar Lipids) was added as an internal standard. Lipids were resolved and detected by ultra-performance LC on a reverse-phase column (ACQUITY UPLC CSH C18 column, length 100 mm; Waters, Milford, MA) coupled with electrospray ionization tandem triple quadrupole MS (Xevo TQ-S, Waters). The resolving conditions for ultra-performance LC were as follows. The flow rate was 0.4 ml/min in the binary gradient system using mobile phase A [acetonitrile/water (3:2, v/v) containing 10 mM ammonium formate] and mobile phase B [acetonitrile/2-pronanol (9:1, v/v) containing 10 mM ammonium formate]. The elution gradient steps were as follows: 0 min, 40 % B; 0-18 min, gradient to 100% B; 18-23 min, 100% B; 23-23.1 min, gradient to 40% B; 23.1-25 min, 40% B. Lipids were detected by multiple reaction monitoring essentially as described previously (32) by selecting specific *m/z* at quadrupole mass filters Q1 and Q3 (Tables S1 and S2). Data were analyzed and quantified using MassLynx software (Waters).

Immunoblotting. Total lysates were prepared from yeast as described previously (47). Immunoblotting was performed as described previously (34) using anti-FLAG M2 (1 μg/ml; Agilent Technologies, Santa Clara, CA), anti-Pgk1 (0.5 μg/ml; Thermo Fisher Scientific), anti-GAPDH (1:1,000 dilution; Thermo Fisher Scientific), and anti-calnexin PM060 (1:1,000

dilution; Medical & Biological Laboratories, Nagoya, Japan) antibodies as the primary antibody and HRP-conjugated anti-mouse or anti-rabbit IgG $F(ab')_2$ fragment (1:7,500 dilution; GE Healthcare Life Sciences, Little Chalfont, UK) as the secondary antibody. Immunodetection was performed using the Pierce ECL Western Blotting Substrate (Thermo Fisher Scientific). In some cases, the contrast of the images was enhanced through linear adjustment using Photoshop CS6 software (Adobe).

Indirect Immunofluorescence Microscopy. Indirect immunofluorescence microscopy was performed as described previously (34) using anti-FLAG (1:1,000 dilution), anti-calnexin 4F10 (1:500 dilution; Medical & Biological Laboratories), and anti-Grp75 30A5 (1/200 dilution; Nventa Biopharmaceuticals, San Diego, CA) antibodies as the primary antibody. Rabbit anti-FLAG polyclonal antibody was raised against a peptide (NH_2-MDYKDHDGDYKDHDIDYKDDDDKC-COOH). Alexa Fluor 488-conjugated anti-rabbit antibody or Alexa Fluor 594-conjugated anti-mouse antibody (each at 5 μg/ml; Thermo Fisher Scientific) was used as the secondary antibody.

Real-Time Quantitative RT-PCR. Total RNA was isolated from CHO-K1 cells, HeLa cells, and human keratinocytes differentiated for seven days, using a NucleoSpin RNA II kit (MACHERY-NAGEL, Dueren, Germany), according to the manufacturer's instructions. The obtained mRNAs were converted to cDNAs using PrimeScript™ II Reverse Transcriptase (TAKARA Bio). Other human cDNAs were purchased from Takara Bio (Human MTC Multiple Tissue cDNA Panels I and II). Real-time quantitative PCR was performed using One-Step SYBR PrimeScript RT-PCR Kit II (Takara Bio) and primers (for human *GAPDH*, 5'-CAACAGCGACACCCACTCCTCCACC-3' and 5'-

ATACCAGGAAATGAGCTTGACAAAG-3'; for human *HACL1*, 5'-GCCAAATTCACATTATGAGCAAGTC-3' and 5'-TTACATATTAGAGCGGGTCAGCCAA-3'; for human *HACL2*, 5'-GTTTGGGGACGGAGCTTTTGGCTAC-3' and 5'-GATGTTGACCACAACCGGGTGGCCG-3'; for Chinese hamster *Gapdh*, 5'-CAAGTATGAGGACATCAAGAAGGTG-3' and 5'-TTACTCCTTGGAGGCCATGTAGGCC-3'; for Chinese hamster *Hacl1*, 5'-TAAACAATAATGGAATCTACCAAGG-3' and 5'-TCACATGTTAGAACGGGTGAGCCAG-3'; and for Chinese hamster *Hacl2*, 5'-CTACAGCCTCATCGAGTTTGACACA-3' and 5'-AAATCTGTCCTCCCGATCAGGATGT-3') on a CFX96 Touch real-time PCR detection system (Bio-Rad Laboratories, Hercules, CA), according to the manufacturer's instructions. The gene amplification efficiencies of the primers used in this study were all >90%. The gene expression levels were normalized with those of *GAPDH*/*Gapdh*. The reaction was conducted by incubating the samples at 95 °C for 3 min, followed by 39 cycles of incubation at 95 °C for 10 s, 55 °C for 30 s, and 72 °C for 30 s.

Footnotes

T.K. designed and performed the research and analyzed the data. N.S. prepared [^{3}H]2-OH C16:0-COOH. A.K. planned the project, designed the research, and wrote the paper.

The authors declare no conflict of interest.

Acknowledgments

We are grateful to Dr. Raphael A. Zoeller (Boston University School of Medicine) for providing FAA-K1A cells. This work was supported by funding from Advanced Research and Development Programs for Medical Innovation (AMED-CREST; awarded to A.K.) from the Japan Agency for Medical Research and Development (AMED), by a Grant-in-Aid for Scientific Research (A) 26251010 (awarded to A.K.) from the Japan Society for the Promotion of Science (JSPS), and by a Grant-in-Aid for JSPS Fellows (02202; awarded to T.K.) from JSPS.

References

1. Eaton S, Bartlett K, Pourfarzam M (1996) Mammalian mitochondrial β-oxidation. *Biochem J* 320:345-357.
2. Wanders RJ (2004) Peroxisomes, lipid metabolism, and peroxisomal disorders. *Mol Genet Metab* 83(1-2):16-27.
3. Foulon V, et al. (2005) Breakdown of 2-hydroxylated straight chain fatty acids via peroxisomal 2-hydroxyphytanoyl-CoA lyase: a revised pathway for the α-oxidation of straight chain fatty acids. *J Biol Chem* 280(11):9802-9812.
4. Casteels M, Sniekers M, Fraccascia P, Mannaerts GP, Van Veldhoven PP (2007) The role of 2-hydroxyacyl-CoA lyase, a thiamin pyrophosphate-dependent enzyme, in the peroxisomal metabolism of 3-methyl-branched fatty acids and 2-hydroxy straight-chain fatty acids. *Biochem Soc Trans* 35(Pt 5):876-880.
5. Smith S, Witkowski A, Joshi AK (2003) Structural and functional organization of the animal fatty acid synthase. *Prog Lipid Res* 42(4):289-317.
6. Kihara A (2012) Very long-chain fatty acids: elongation, physiology and related disorders. *J Biochem* 152(5):387-395.
7. Sassa T, Kihara A (2014) Metabolism of very long-chain fatty acids: genes and pathophysiology. *Biomol Ther* 22(2):83-92.
8. Mead JF, Levis GM (1963) A 1 carbon degradation of the long chain fatty acids of brain sphingolipids. *J Biol Chem* 238:1634-1636.
9. Levis GM, Mead JF (1964) An α-hydroxy acid decarboxylase in brain microsomes. *J Biol Chem* 239:77-80.

10. Kihara A, Mitsutake S, Mizutani Y, Igarashi Y (2007) Metabolism and biological functions of two phosphorylated sphingolipids, sphingosine 1-phosphate and ceramide 1-phosphate. *Prog Lipid Res* 46(2):126-144.

11. Kihara A (2016) Synthesis and degradation pathways, functions, and pathology of ceramides and epidermal acylceramides. *Prog Lipid Res* 63:50-69.

12. Hama H (2010) Fatty acid 2-hydroxylation in mammalian sphingolipid biology. *Biochim Biophys Acta* 1801(4):405-414.

13. Svennerholm L, Ställberg-Stenhagen S (1968) Changes in the fatty acid composition of cerebrosides and sulfatides of human nervous tissue with age. *J Lipid Res* 9(2):215-225.

14. Farwanah H, Wohlrab J, Neubert RH, Raith K (2005) Profiling of human stratum corneum ceramides by means of normal phase LC/APCI-MS. *Anal Bioanal Chem* 383(4):632-637.

15. Bowen DM, Radin NS (1968) Hydroxy fatty acid metabolism in brain. *Adv Lipid Res* 6:255-272.

16. Zöller I, et al. (2008) Absence of 2-hydroxylated sphingolipids is compatible with normal neural development but causes late-onset axon and myelin sheath degeneration. *J Neurosci* 28(39):9741-9754.

17. Alderson NL, et al. (2004) The human *FA2H* gene encodes a fatty acid 2-hydroxylase. *J Biol Chem* 279(47):48562-48568.

18. Edvardson S, et al. (2008) Mutations in the fatty acid 2-hydroxylase gene are associated with leukodystrophy with spastic paraparesis and dystonia. *Am J Hum Genet* 83(5):643-648.

19. Dick KJ, et al. (2010) Mutation of FA2H underlies a complicated form of hereditary spastic paraplegia (SPG35). *Hum Mutat* 31(4):E1251-1260.

20. Potter KA, et al. (2011) Central nervous system dysfunction in a mouse model of FA2H deficiency. *Glia* 59(7):1009-1021.

21. Nakahara K, et al. (2012) The Sjögren-Larsson syndrome gene encodes a hexadecenal dehydrogenase of the sphingosine 1-phosphate degradation pathway. *Mol Cell* 46(4):461-471.

22. Ohkuni A, Ohno Y, Kihara A (2013) Identification of acyl-CoA synthetases involved in the mammalian sphingosine 1-phosphate metabolic pathway. *Biochem Biophys Res Commun* 442(3-4):195-201.

23. Wakashima T, Abe K, Kihara A (2014) Dual functions of the *trans*-2-enoyl-CoA reductase TER in the sphingosine 1-phosphate metabolic pathway and in fatty acid elongation. *J Biol Chem* 289(36):24736-24748.

24. Vogel P, et al. (2009) Incomplete inhibition of sphingosine 1-phosphate lyase modulates immune system function yet prevents early lethality and non-lymphoid lesions. *PLoS One* 4(1):e4112.

25. Bektas M, et al. (2010) Sphingosine 1-phosphate lyase deficiency disrupts lipid homeostasis in liver. *J Biol Chem* 285(14):10880-10889.

26. Ishikawa J, et al. (2010) Changes in the ceramide profile of atopic dermatitis patients. *J Invest Dermatol* 130(10):2511-2514.

27. Kondo N, et al. (2014) Identification of the phytosphingosine metabolic pathway leading to odd-numbered fatty acids. *Nat Commun* 5:5338.

28. Jansen GA, Wanders RJ (2006) Alpha-oxidation. *Biochim Biophys Acta* 1763(12):1403-1412.

29. Foulon V, et al. (1999) Purification, molecular cloning, and expression of 2-hydroxyphytanoyl-CoA lyase, a peroxisomal thiamine pyrophosphate-dependent enzyme that catalyzes the carbon-carbon bond cleavage during α-oxidation of 3-methyl-branched fatty acids. *Proc Natl Acad Sci USA* 96(18):10039-10044.

30. Rizzo WB (2007) Sjögren-Larsson syndrome: molecular genetics and biochemical pathogenesis of fatty aldehyde dehydrogenase deficiency. *Mol Genet Metab* 90(1):1-9.

31. James PF, Zoeller RA (1997) Isolation of animal cell mutants defective in long-chain fatty aldehyde dehydrogenase. Sensitivity to fatty aldehydes and Schiff's base modification of phospholipids: implications for Sjögren-Larsson syndrome. *J Biol Chem* 272(38):23532-23539.

32. Naganuma T, et al. (2016) Disruption of the Sjögren-Larsson syndrome gene *Aldh3a2* in mice increases keratinocyte growth and retards skin barrier recovery. *J Biol Chem* 291(22):11676-11688.

33. Kitamura T, et al. (2013) Substrate specificity, plasma membrane localization, and lipid modification of the aldehyde dehydrogenase ALDH3B1. *Biochim Biophys Acta* 1831(8):1395-1401.

34. Kitamura T, Takagi S, Naganuma T, Kihara A (2015) Mouse aldehyde dehydrogenase ALDH3B2 is localized to lipid droplets via two C-terminal tryptophan residues and lipid modification. *Biochem J* 465(1):79-87.

35. Ashibe B, Hirai T, Higashi K, Sekimizu K, Motojima K (2007) Dual subcellular localization in the endoplasmic reticulum and peroxisomes and a vital role in protecting against oxidative stress of fatty aldehyde dehydrogenase are achieved by alternative splicing. *J Biol Chem* 282(28):20763-20773.

36. Liu H, et al. (2000) Molecular cloning and functional characterization of a novel mammalian sphingosine kinase type 2 isoform. *J Biol Chem* 275(26):19513-19520.

37. Kohama T, et al. (1998) Molecular cloning and functional characterization of murine sphingosine kinase. *J Biol Chem* 273(37):23722-23728.

38. Watkins PA, Maiguel D, Jia Z, Pevsner J (2007) Evidence for 26 distinct acyl-coenzyme A synthetase genes in the human genome. *J Lipid Res* 48(12):2736-2750.

39. Soupene E, Kuypers FA (2008) Mammalian long-chain acyl-CoA synthetases. *Exp Biol Med (Maywood)* 233(5):507-521.

40. Ikeda M, Kihara A, Igarashi Y (2004) Sphingosine-1-phosphate lyase SPL is an endoplasmic reticulum-resident, integral membrane protein with the pyridoxal 5'-phosphate binding domain exposed to the cytosol. *Biochem Biophys Res Commun* 325(1):338-343.

41. Eckhardt M, Yaghootfam A, Fewou SN, Zoller I, Gieselmann V (2005) A mammalian fatty acid hydroxylase responsible for the formation of α-hydroxylated galactosylceramide in myelin. *Biochem J* 388(Pt 1):245-254.

42. Michaelson LV, Napier JA, Molino D, Faure JD (2016) Plant sphingolipids: Their importance in cellular organization and adaption. *Biochim Biophys Acta* 1861(9 Pt B):1329-1335.

43. Winzeler EA, et al. (1999) Functional characterization of the *S. cerevisiae* genome by gene deletion and parallel analysis. *Science* 285(5429):901-906.

44. Ikeda M, et al. (2008) Characterization of four mammalian 3-hydroxyacyl-CoA dehydratases involved in very long-chain fatty acid synthesis. *FEBS Lett* 582(16):2435-2440.

45. Ohno Y, et al. (2009) Palmitoylation of the sphingosine 1-phosphate receptor S1P is involved in its signaling functions and internalization. *Genes Cells* 14(8):911-923.

46. Kihara A, Kurotsu F, Sano T, Iwaki S, Igarashi Y (2005) Long-chain base kinase Lcb4 is anchored to the membrane through its palmitoylation by Akr1. *Mol Cell Biol* 25(21):9189-9197.

47. Kihara A, Igarashi Y (2002) Identification and characterization of a *Saccharomyces cerevisiae* gene, *RSB1*, involved in sphingoid long-chain base release. *J Biol Chem* 277(33):30048-30054.

Figure Legends

Fig. 1. ALDH3A2 is involved in the first oxidation reaction of the PHS degradation pathway. (*A*) CHO-K1 and the *Aldh3a2*-deficient FAA-K1A cells were labeled with 0.1 μCi (2.25 nmol) [^{3}H]DHS or [^{3}H]PHS for 5 h at 37 °C. Lipids were extracted, treated with or without alkaline solution, and separated by normal-phase TLC with 1-butanol/acetic acid/water (3:1:1, v/v). A solid circle and triangle represent PlsE and 2-OH PlsE, respectively. They are converted to the corresponding A-GPE or 2-OH A-GPE and other breakdown products (A-GPE' or 2-OH A-GPE') by alkaline treatment (open circles and triangles). Solid and open squares indicate PlsC and A-GPC, respectively. (*B*) CHO-K1 and FAA-K1A cells were treated with ethanol or 0.8 μM PHS for 24 h at 37 °C. Lipids were extracted, and C16:0 CER species were analyzed by LC-MS/MS. Values represent the means ± S.D. from three independent reactions. Statistically significant differences are indicated (*, $P < 0.05$; Tukey's test).

Fig. 2. HACL2 is a 2-OH acyl-CoA lyase catalyzing conversion of 2-OH acyl-CoA to fatty aldehyde. (*A* and *B*) Yeast cells (4378; *mpo1*Δ) bearing the pAKNF316 (vector), pNK46 (*3xFLAG-MPO1*), pZKN14 (*3xFLAG-HACL2*), or pTK183 (*3xFLAG-HACL1*) plasmid were labeled with 0.1 μCi [^{3}H]PHS for 3 h at 30 °C. Lipids were extracted and separated by normal-phase TLC with chloroform/methanol/4.2 M ammonia (9:7:2, v/v) (*A*). Total lysates were prepared and subjected to immunoblotting with anti-FLAG antibody and, to demonstrate equal protein loading, anti-Pgk1 (3-phosphoglycerate kinase) antibody (*B*). (*C* and *D*) Affinity-purified, 3xFLAG-tagged HACL1 and HACL2 proteins (1 μg) were incubated with 100 μM 2-OH C18:0-COOH (2-OH C18 FA; *C*) or 2-OH C18:0-CoA (2-OH C18-CoA; *C* and *D*) at 37 °C for 4 h in the presence (*C* and *D*) or absence (*D*) of 20 μM TPP.

After the reaction, lipids were extracted, separated by normal-phase TLC together with the standard C16:0-CHO (10 nmol), and stained with Schiff reagent.

Fig. 3. HACL2 is a major 2-OH acyl-CoA lyase involved in the PHS degradation pathway. (*A*) Total RNAs were prepared from CHO-K1 cells and subjected to real-time quantitative RT-PCR using specific primers for *Hacl1*, *Hacl2*, and *Gapdh*. Values represent the means ± S.D. relative to *Gapdh* expression levels from three independent reactions. A statistically significant difference is indicated (*, $P < 0.05$; Student's t-test). (*B*) Wild type, *Hacl1* KO, *Hacl2* KO, and *Hacl1 Hacl2* DKO CHO-K1 cells were labeled with 0.2 μCi [^{3}H]PHS for 4 h at 37 °C. Lipids were extracted, treated with or without alkaline solution, and separated by normal-phase TLC with 1-butanol/acetic acid/water (3:1:1, v/v). (*C* and *D*) Wild type, *Hacl1* KO, *Hacl2* KO, and *Hacl1 Hacl2* DKO CHO-K1 cells were treated with ethanol or 5 μM 2-OH C16:0-COOH (C16:0 FA; Wako Pure Chemical Industries) for 24 h at 37 °C. Lipids were extracted, and odd-numbered PC (*C*) and even-numbered PC (*D*) species were analyzed by LC-MS/MS. Values represent the means ± S.D. of total levels of odd-numbered (*C*) or even-numbered PCs (*D*) from three independent reactions. Statistically significant differences are indicated (*, $P < 0.05$; Tukey's test).

Fig. 4. HACL2 is an ER membrane protein. (*A* and *B*) HeLa cells were transfected with the pCE-puro 3xFLAG-HACL1 or pCE-puro HACL2-3xFLAG plasmid and cultured for 24 h at 37 °C. (*A*) Cells were visualized by indirect immunofluorescence microscopy with anti-FLAG plus anti-calnexin (ER marker) antibodies or anti-FLAG plus anti-Grp75 (mitochondria marker) antibodies. Bar, 25 μm. (*B*) Total lysates were prepared and subjected to centrifugation at 100,000 g for 30 min. The resulting supernatant (soluble fraction; S) and

pellet (membrane fraction; M) were separated by SDS-PAGE and detected by immunoblotting with anti-FLAG, anti-GAPDH (soluble protein marker), and anti-calnexin (membrane protein marker) antibodies. (*C*) Human tissue cDNAs and cDNAs prepared from keratinocytes differentiated (dif.) for 7 days were subjected to real-time quantitative RT-PCR using specific primers for *HACL1*, *HACL2*, and *GAPDH*. Values represent the means ± S.D. relative to *GAPDH* expression levels from three independent reactions.

Fig. 5. ALDH3A2 catalyzes the second oxidation step of the PHS degradation pathway. (*A*) CHO-K1, FAA-K1A (*Aldh3a2*-deficient), and FAA-ALDH3A2 (FAA-K1A cells stably expressing *3xFLAG-ALDH3A2*; FAA-A2) cells were labeled with 0.2 μCi [^{3}H]C16:0-COOH (C16:0 FA) or [^{3}H]2-OH C16:0-COOH (2-OH C16:0 FA) for 4 h at 37 °C. Lipids were extracted, treated with or without alkaline solution, and separated by normal-phase TLC with 1-butanol/acetic acid/water (3:1:1, v/v). A solid circle represents PlsE, which is converted to A-GPE and other breakdown products (A-GPE') by alkaline treatment (open circles). Solid and open squares indicate PlsC and A-GPC, respectively. (*B* and *C*) CHO-K1, FAA-K1A, and FAA-ALDH3A2 (FAA-A2) cells were treated with ethanol or 5 μM 2-OH C16:0-COOH for 24 h at 37 °C. Lipids were extracted, and odd-numbered PC (*B*) and even-numbered PC (*C*) species were analyzed by LC-MS/MS. Values represent the means ± S.D. of total levels of odd-numbered (*B*) and even-numbered (*C*) PCs from three independent reactions. Statistically significant differences are indicated (*, $P < 0.05$; Tukey's test).

Fig. 6. PHS metabolic pathway. PHS is metabolized to either complex sphingolipids as an LCB component or to glycerolipids as a FA component via the PHS degradation pathway. In the degradation pathway, PHS is phosphorylated to PHS 1-phosphate by the SPH kinase

SPHK2, cleaved to 2-OH C16:0-CHO by the SPH 1-phosphate lyase SPGL1, oxidized to 2-OH C16:0-COOH by the FALDH ALDH3A2, and converted to 2-OH C16:0-CoA by ACSs. Most of the generated 2-OH C16:0-CoAs are subjected to C1 removal by 2-OH acyl-CoA lyases (mainly by HACL2 and partly by HACL1), producing C15:0-CHO. Some 2-OH C16:0-CoAs are incorporated into sphingolipids as a FA moiety. C15:0-CHO is oxidized to C15:0-COOH by the FALDH ALDH3A2, converted to C15:0-CoA by ACSs, and incorporated into glycerolipids.

SI Figure Legends

Fig. S1. DHS and SPH degradation pathways. (*A*) Structures of DHS, SPH, and their metabolites and their structural symbols are depicted. (*B*) DHS and SPH degradation pathways leading to ester-linked glycerolipids and the involved genes are illustrated.

Fig. S2. DHS and PHS metabolic pathways. (*A*) Structures of PHS and its metabolites as well as the structural symbols of LCB metabolites are depicted. (*B* and *C*) The known DHS metabolic pathway (*B*), and the expected PHS metabolic pathway (*C*), leading to complex sphingolipids and ether- and ester-linked glycerolipids along with the involved genes are illustrated. Dashed lines represent minor metabolic routes. Pink arrows represent usually minor routes that are major routes in *Aldh3a2*-deficient cells. GSL, glycosphingolipid.

Fig. S3. Schematic representation of the mutations in the *Hacl* KO cells used in this study. Gene structures of *Hacl1* and *Hacl2* as well as the gene mutations in *Hacl1* KO (A), *Hacl2* KO (B), and *Hacl1 Hacl2* DKO (C) cells are represented. Blue and red nucleotides are PAM sequences and mutated nucleotides, respectively. Underlines indicate guide RNAs.

Fig. S4. Normal DHS metabolism in *Hacl* mutant cells. Wild type, *Hacl1* KO, *Hacl2* KO, and *Hacl1 Hacl2* DKO CHO-K1 cells were labeled with 0.2 μCi [^{3}H]DHS for 4 h at 37 °C. Lipids were extracted, treated with or without alkaline solution, and separated by normal-phase TLC with 1-butanol/acetic acid/water (3:1:1, v/v).

Fig. S5. Predicted PHS degradation pathway. The PHS degradation pathway depicted in Fig. S2*C* was updated to consider the results of Figs. 1-3. Dashed lines represent minor

metabolic routes. Pink arrows represent usually minor routes that are major routes in *Aldh3a2*-deficient cells. GSL, glycosphingolipid.

Fig. S6. HACL1 and HACL2 are redundantly involved in the conversion of 2-OH C16:0-COOH to odd-numbered PCs. (*A* and *B*) Detailed results of Fig. 3*C* and *D*. Wild type, *Hacl1* KO, *Hacl2* KO, and *Hacl1 Hacl2* DKO CHO-K1 cells were treated with ethanol or 5 μM 2-OH C16:0-COOH (C16:0 FA) for 24 h at 37 °C. Lipids were extracted, and odd-numbered (*A*) and even-numbered PC (*B*) species were analyzed by LC-MS/MS. Values represent the means ± S.D. of odd-numbered (*A*) and even-numbered (*B*) PC species that have the indicated chain-lengths from three independent reactions. Statistically significant differences are indicated (*, $P < 0.05$; Tukey's test).

Fig. S7. ALDH3A2 is involved in the conversion of 2-OH C16:0-COOH to odd-numbered PCs. (*A* and *B*) Detailed results of Fig. 5*B* and *C*. CHO-K1, FAA-K1A (*Aldh3a2*-deficient), and FAA-ALDH3A2 (FAA-K1A cells stably expressing *3xFLAG-ALDH3A2*) cells were treated with ethanol or 5 μM 2-OH C16:0-COOH for 24 h at 37 °C. Lipids were extracted, and odd-numbered (*A*) and even-numbered PC (*B*) species were analyzed by LC-MS/MS. Values represent the means ± S.D. of odd-numbered (*A*) and even-numbered (*B*) PC species that have the indicated chain-lengths from three independent reactions. Statistically significant differences are indicated (*, $P < 0.05$; Tukey's test).

Table S1. Selected *m/z* values for CERs.

C16 CERs	Precursor ions (Q1)		Product ion (Q3)
	$[M-H_2O+H]^+$	$[M+H]^+$	
CER	520.2	538.2	264.2
PHS-CER	538.4	556.4	300.2
2-OH CER	536.15	554.15	264.2
2-OH PHS-CER	554.14	572.15	300.2

Table S2. Selected *m/z* values for PCs.

PCs	Precursor ion (Q1) $[M+HCOO]^-$	Product ions (Q3)	
C12:0/C12:0[a]	666.2	198.9	
C15:0/C16:1	762.3	241.04	253.04
C15:0/C16:0	764.3	241.04	255.04
C15:0/C18:1	764.3	241.04	281.0
C17:0/C18:1	818.3	269.04	281.0
C16:1/C16:0	776.3	253.04	255.04
C16:0/C16:0	778.3	255.04	
C16:1/C18:1	802.3	253.04	281.0
C16:0/C18:1	804.3	255.04	281.0
C18:1/C18:1	830.3	281.0	
C18:0/C18:1	832.2	281.0	283.0

[a]Internal control

Fig. 1

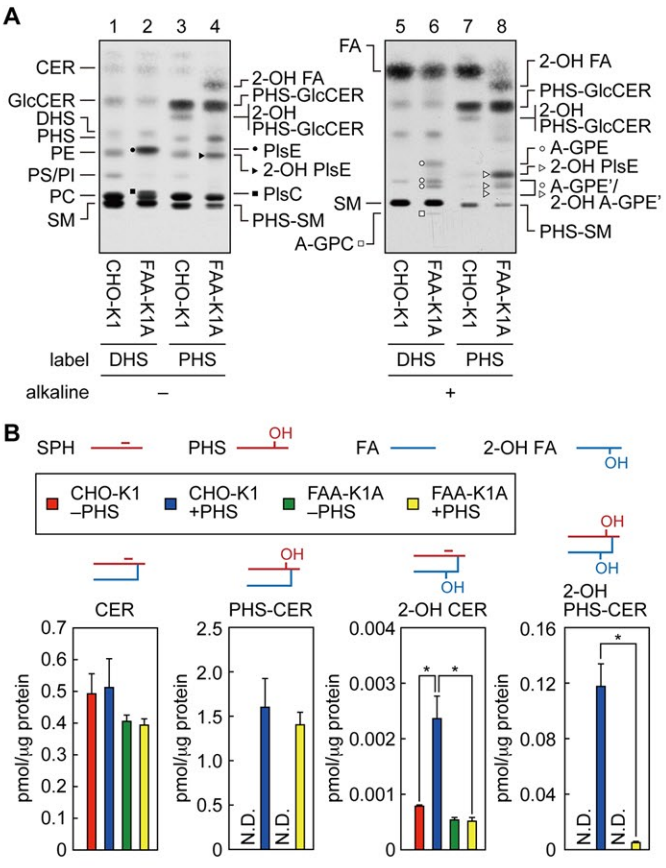
A
1 2 3 4
5 6 7 8
CER
GlcCER
DHS
PHS
PE
PS/PI
PC
SM
2-OH FA
PHS-GlcCER
2-OH PHS-GlcCER
PlsE
2-OH PlsE
PlsC
PHS-SM
FA
SM
A-GPC
2-OH FA
PHS-GlcCER
2-OH PHS-GlcCER
A-GPE
2-OH PlsE
A-GPE'/ 2-OH A-GPE'
PHS-SM
CHO-K1
FAA-K1A
CHO-K1
FAA-K1A
label
DHS
PHS
alkaline
–
+
B
SPH
PHS
FA
2-OH FA
OH
CHO-K1 –PHS
CHO-K1 +PHS
FAA-K1A –PHS
FAA-K1A +PHS
CER
PHS-CER
2-OH CER
2-OH PHS-CER
pmol/μg protein
N.D.
N.D.
*
*
*

Fig. 2

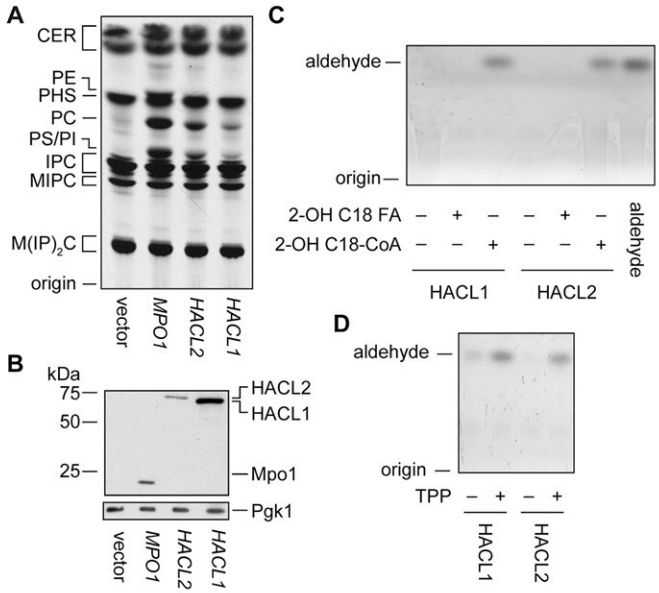
A
CER
PE
PHS
PC
PS/PI
IPC
MIPC
M(IP)2C
origin
vector
MPO1
HACL2
HACL1
B
kDa
75
50
25
HACL2
HACL1
Mpo1
Pgk1
vector
MPO1
HACL2
HACL1
C
aldehyde
origin
2-OH C18 FA – + – – + –
2-OH C18-CoA – – + – – +
aldehyde
HACL1
HACL2
D
aldehyde
origin
TPP – + – +
HACL1
HACL2

Fig. 3

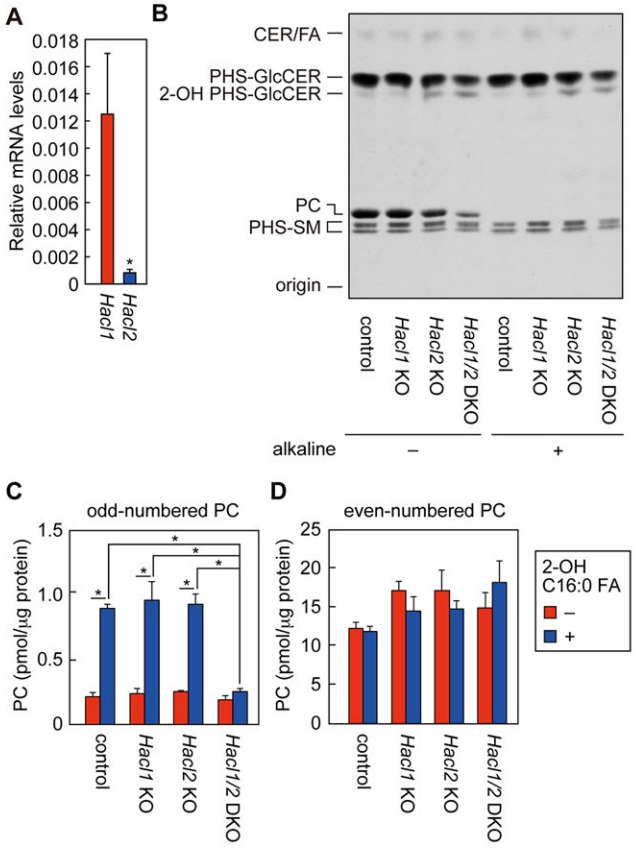
A
Relative mRNA levels
0.018
0.016
0.014
0.012
0.010
0.008
0.006
0.004
0.002
0
*
Hacl1
Hacl2
B
CER/FA
PHS-GlcCER
2-OH PHS-GlcCER
PC
PHS-SM
origin
control
Hacl1 KO
Hacl2 KO
Hacl1/2 DKO
control
Hacl1 KO
Hacl2 KO
Hacl1/2 DKO
alkaline
–
+
C
odd-numbered PC
PC (pmol/μg protein)
1.5
1.0
0.5
0
control
Hacl1 KO
Hacl2 KO
Hacl1/2 DKO
D
even-numbered PC
PC (pmol/μg protein)
25
20
15
10
5
0
control
Hacl1 KO
Hacl2 KO
Hacl1/2 DKO
2-OH
C16:0 FA
–
+

Fig. 4

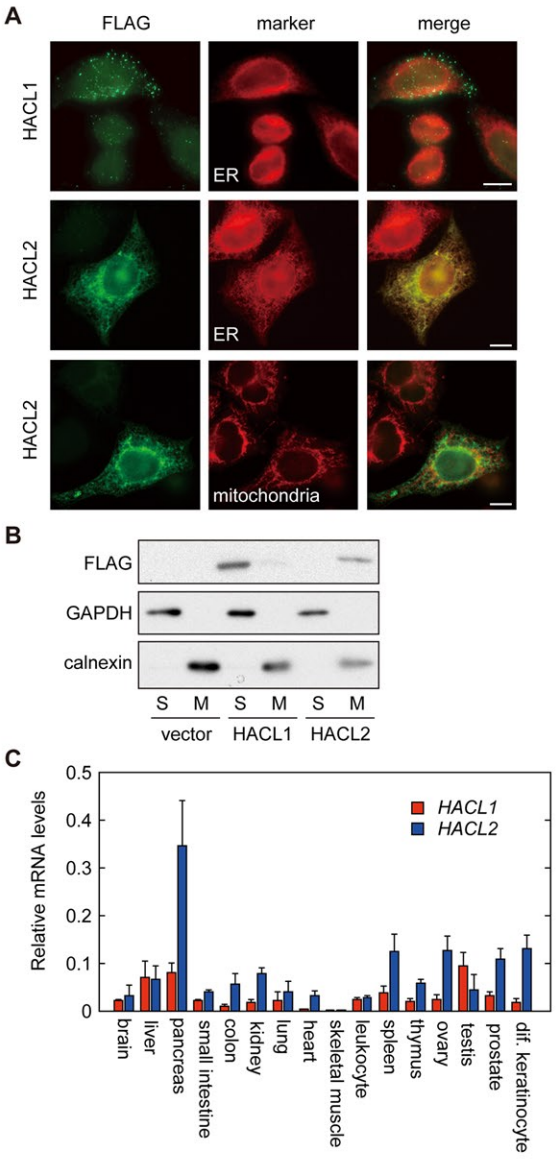
A
FLAG
marker
merge
HACL1
ER
HACL2
ER
HACL2
mitochondria
B
FLAG
GAPDH
calnexin
S M S M S M
vector HACL1 HACL2
C
Relative mRNA levels
0.5
0.4
0.3
0.2
0.1
0
HACL1
HACL2
brain
liver
pancreas
small intestine
colon
kidney
lung
heart
skeletal muscle
leukocyte
spleen
thymus
ovary
testis
prostate
dif. keratinocyte

Fig. 5

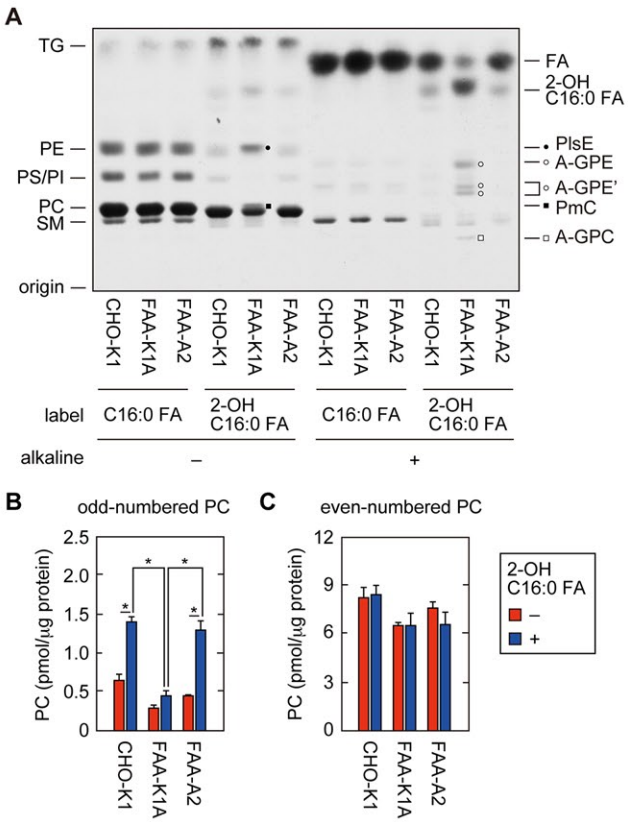
A
TG
PE
PS/PI
PC
SM
origin
FA
2-OH C16:0 FA
PlsE
A-GPE
A-GPE'
PmC
A-GPC
CHO-K1
FAA-K1A
FAA-A2
label
C16:0 FA
2-OH C16:0 FA
alkaline
–
+
B
odd-numbered PC
PC (pmol/μg protein)
C
even-numbered PC
2-OH C16:0 FA

Fig. 6

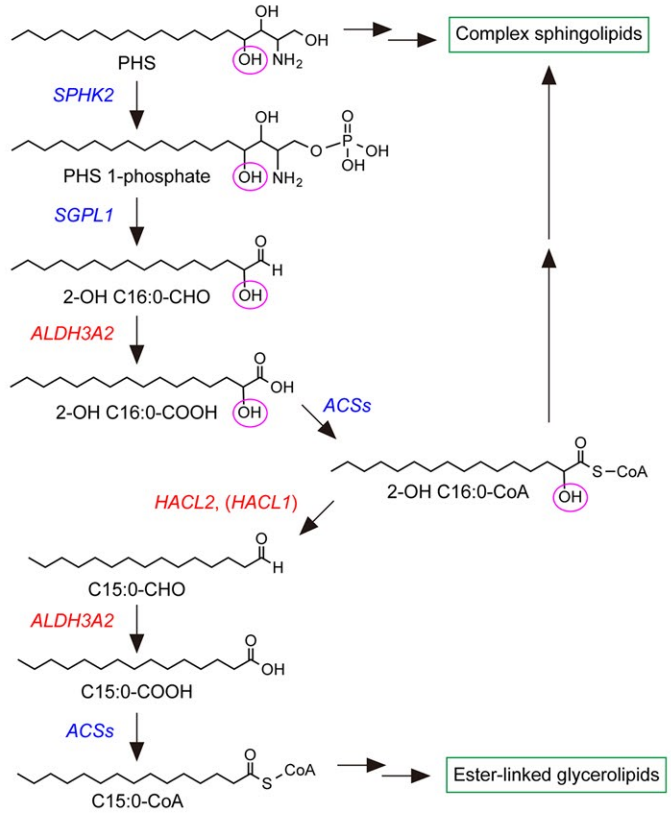
PHS
Complex sphingolipids
SPHK2
PHS 1-phosphate
SGPL1
2-OH C16:0-CHO
ALDH3A2
2-OH C16:0-COOH
ACSs
2-OH C16:0-CoA
HACL2, (HACL1)
C15:0-CHO
ALDH3A2
C15:0-COOH
ACSs
C15:0-CoA
Ester-linked glycerolipids

Fig. S1

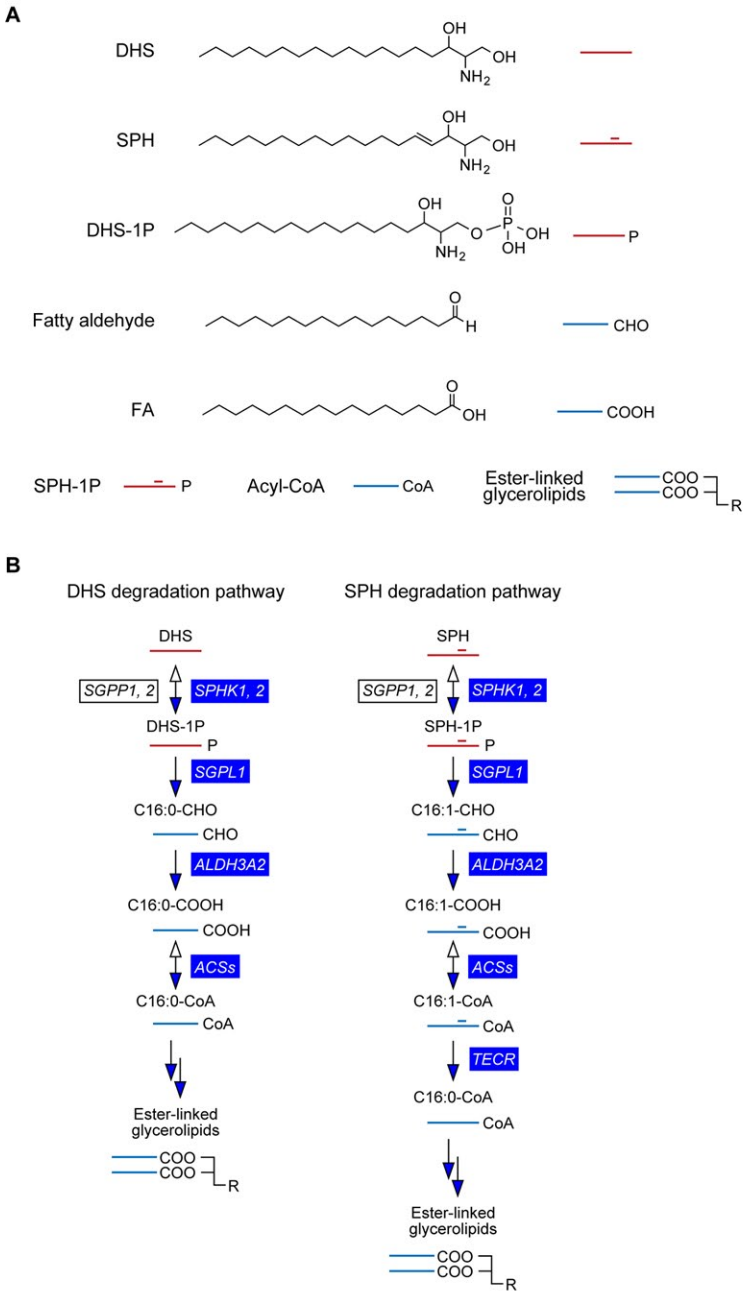
A
DHS
SPH
DHS-1P
Fatty aldehyde
FA
SPH-1P
P
Acyl-CoA
CoA
Ester-linked glycerolipids
COO
COO
R
CHO
COOH
B
DHS degradation pathway
SPH degradation pathway
DHS
SPH
SGPP1, 2
SPHK1, 2
DHS-1P
SPH-1P
SGPL1
C16:0-CHO
C16:1-CHO
ALDH3A2
C16:0-COOH
C16:1-COOH
ACSs
C16:0-CoA
C16:1-CoA
TECR
C16:0-CoA
Ester-linked glycerolipids

Fig. S2

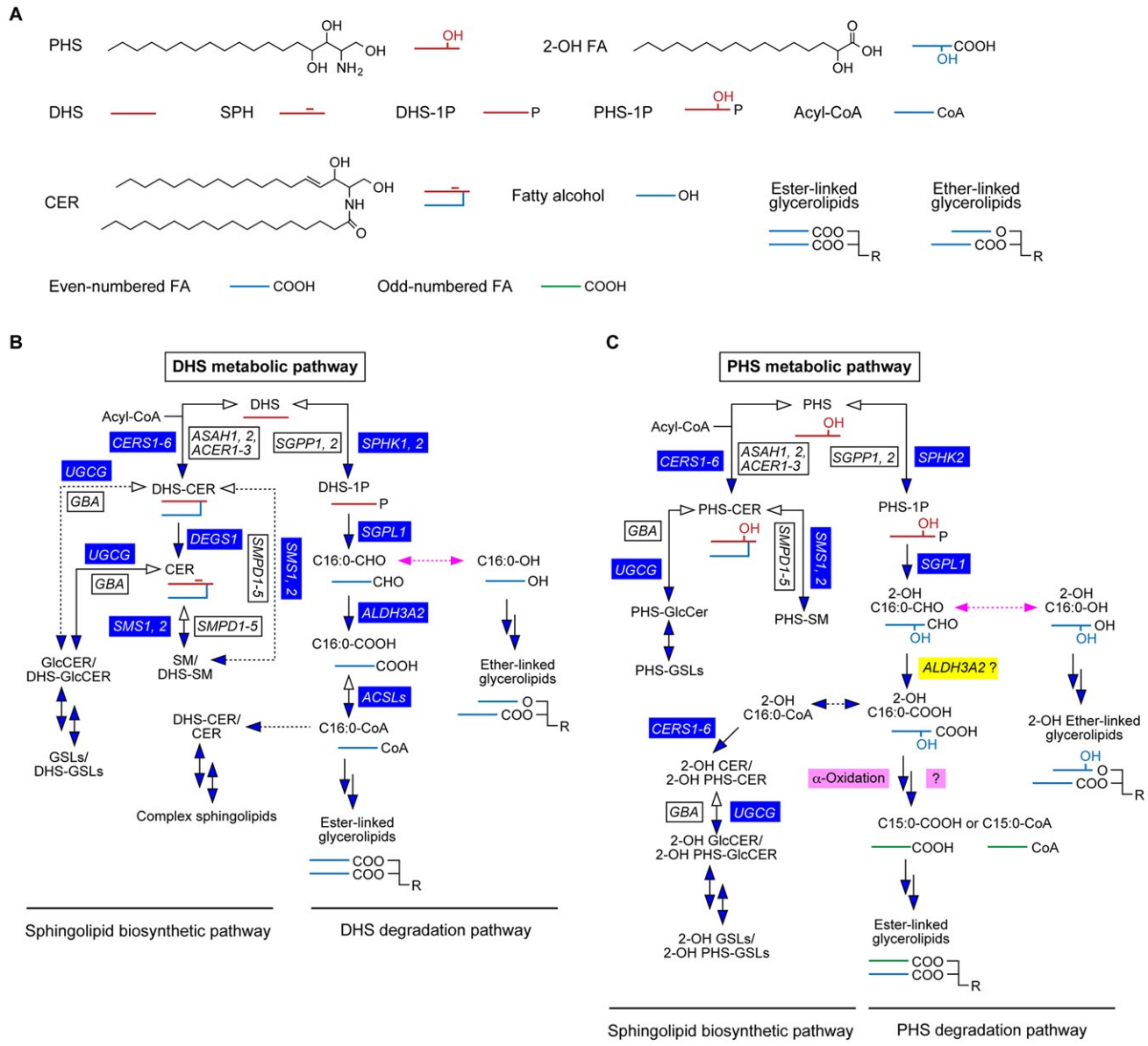
A
PHS
2-OH FA
DHS
SPH
DHS-1P
PHS-1P
Acyl-CoA
CER
Fatty alcohol
Ester-linked glycerolipids
Ether-linked glycerolipids
Even-numbered FA
Odd-numbered FA
B
DHS metabolic pathway
Acyl-CoA
DHS
CERS1-6
ASAH1, 2, ACER1-3
SGPP1, 2
SPHK1, 2
UGCG
GBA
DHS-CER
DHS-1P
DEGS1
SMPD1-5
SMS1, 2
SGPL1
C16:0-CHO
C16:0-OH
CER
CHO
OH
ALDH3A2
C16:0-COOH
COOH
GlcCER/ DHS-GlcCER
SM/ DHS-SM
ACSLs
Ether-linked glycerolipids
DHS-CER/ CER
C16:0-CoA
CoA
GSLs/ DHS-GSLs
Complex sphingolipids
Ester-linked glycerolipids
Sphingolipid biosynthetic pathway
DHS degradation pathway
C
PHS metabolic pathway
PHS
Acyl-CoA
CERS1-6
ASAH1, 2, ACER1-3
SGPP1, 2
SPHK2
PHS-CER
PHS-1P
GBA
UGCG
SMPD1-5
SMS1, 2
SGPL1
PHS-GlcCer
PHS-SM
2-OH C16:0-CHO
2-OH C16:0-OH
PHS-GSLs
ALDH3A2 ?
2-OH C16:0-CoA
2-OH C16:0-COOH
2-OH Ether-linked glycerolipids
2-OH CER/ 2-OH PHS-CER
α-Oxidation
?
2-OH GlcCER/ 2-OH PHS-GlcCER
C15:0-COOH or C15:0-CoA
CoA
2-OH GSLs/ 2-OH PHS-GSLs
Ester-linked glycerolipids
Sphingolipid biosynthetic pathway
PHS degradation pathway

Fig. S3

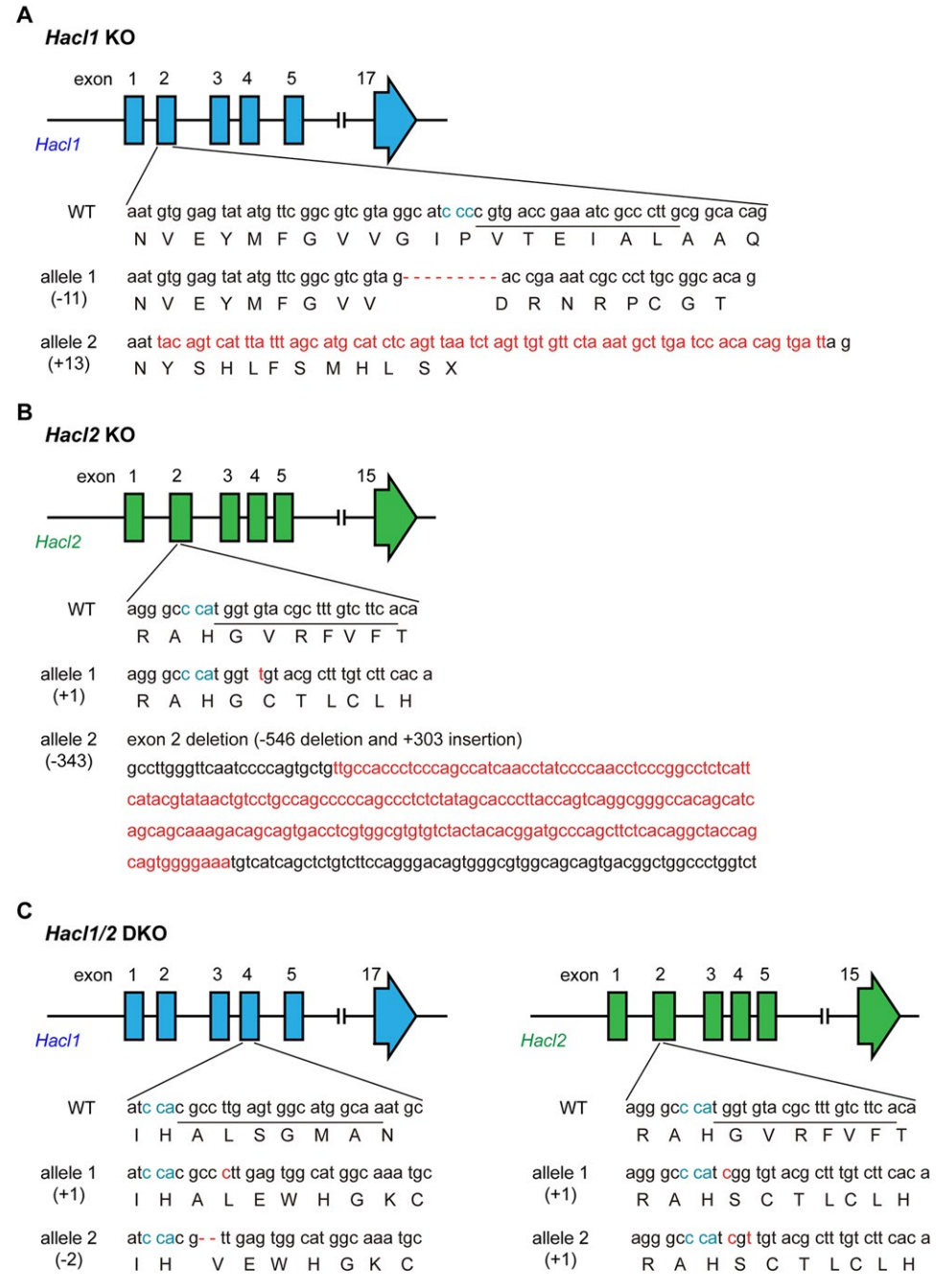
A
Hacl1 KO
exon 1 2 3 4 5 17
Hacl1
WT
aat gtg gag tat atg ttc ggc gtc gta ggc atc ccc gtg acc gaa atc gcc ctt gcg gca cag
N V E Y M F G V V G I P V T E I A L A A Q
allele 1 (-11)
aat gtg gag tat atg ttc ggc gtc gta g- - - - - - - - - ac cga aat cgc cct tgc ggc aca g
N V E Y M F G V V D R N R P C G T
allele 2 (+13)
aat tac agt cat tta ttt agc atg cat ctc agt taa tct agt tgt gtt cta aat gct tga tcc aca cag tga tta g
N Y S H L F S M H L S X
B
Hacl2 KO
exon 1 2 3 4 5 15
Hacl2
WT
agg gcc cat ggt gta cgc ttt gtc ttc aca
R A H G V R F V F T
allele 1 (+1)
agg gcc cat ggt tgt acg ctt tgt ctt cac a
R A H G C T L C L H
allele 2 (-343)
exon 2 deletion (-546 deletion and +303 insertion)
gccttgggttcaatccccagtgctgttgccaccctcccagccatcaacctatccccaacctcccggcctctcatt
catacgtataactgtcctgccagcccccagccctctctatagcacccttaccagtcaggcgggccacagcatc
agcagcaaagacagcagtgacctcgtggcgtgtgtctactacacggatgcccagcttctcacaggctaccag
cagtggggaaatgtcatcagctctgtcttccagggacagtgggcgtggcagcagtgacggctggccctggtct
C
Hacl1/2 DKO
exon 1 2 3 4 5 17
Hacl1
WT
atc cac gcc ttg agt ggc atg gca aat gc
I H A L S G M A N
allele 1 (+1)
atc cac gcc ctt gag tgg cat ggc aaa tgc
I H A L E W H G K C
allele 2 (-2)
atc cac g- - tt gag tgg cat ggc aaa tgc
I H V E W H G K C
exon 1 2 3 4 5 15
Hacl2
WT
agg gcc cat ggt gta cgc ttt gtc ttc aca
R A H G V R F V F T
allele 1 (+1)
agg gcc cat cgg tgt acg ctt tgt ctt cac a
R A H S C T L C L H
allele 2 (+1)
agg gcc cat cgt tgt acg ctt tgt ctt cac a
R A H S C T L C L H

Fig. S4

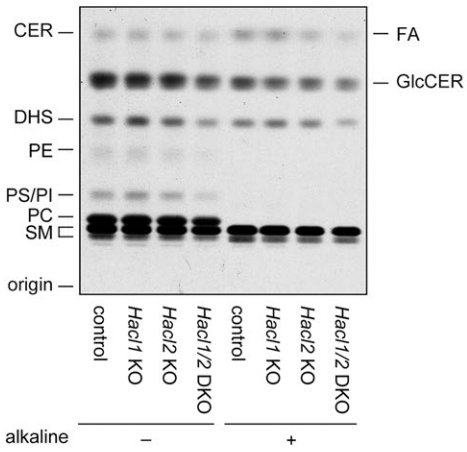
CER
DHS
PE
PS/PI
PC
SM
origin
FA
GlcCER
control
Hac1 KO
Hac2 KO
Hac1/2 DKO
control
Hac1 KO
Hac2 KO
Hac1/2 DKO
alkaline
–
+

Fig. S5

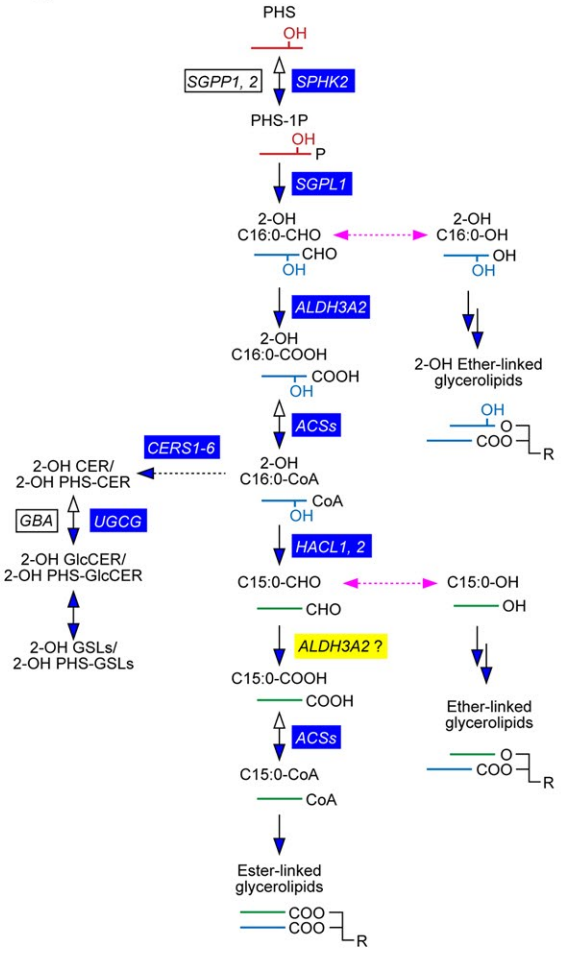
PHS
OH
SGPP1, 2
SPHK2
PHS-1P
OH
P
SGPL1
2-OH
C16:0-CHO
CHO
OH
2-OH
C16:0-OH
OH
OH
ALDH3A2
2-OH
C16:0-COOH
COOH
OH
2-OH Ether-linked
glycerolipids
OH
O
COO
R
ACSs
CERS1-6
2-OH CER/
2-OH PHS-CER
2-OH
C16:0-CoA
CoA
OH
GBA
UGCG
2-OH GlcCER/
2-OH PHS-GlcCER
HACL1, 2
C15:0-CHO
CHO
C15:0-OH
OH
2-OH GSLs/
2-OH PHS-GSLs
ALDH3A2 ?
C15:0-COOH
COOH
Ether-linked
glycerolipids
ACSs
C15:0-CoA
CoA
Ester-linked
glycerolipids
COO
COO
R

Fig. S6

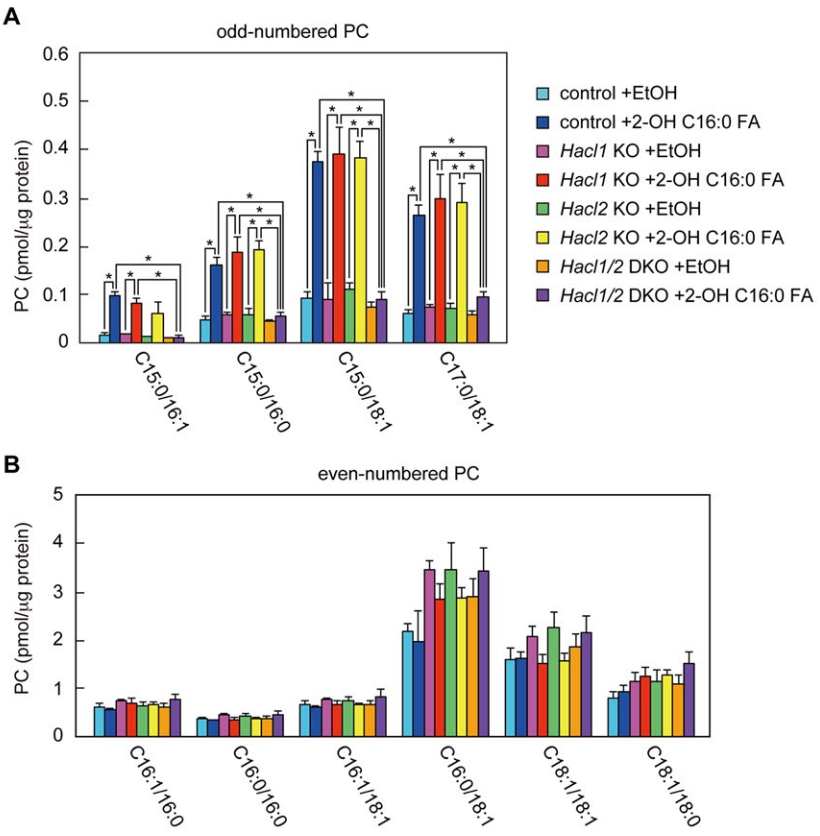
A
odd-numbered PC
PC (pmol/μg protein)
0.6
0.5
0.4
0.3
0.2
0.1
0
C15:0/16:1
C15:0/16:0
C15:0/18:1
C17:0/18:1
control +EtOH
control +2-OH C16:0 FA
Hacl1 KO +EtOH
Hacl1 KO +2-OH C16:0 FA
Hacl2 KO +EtOH
Hacl2 KO +2-OH C16:0 FA
Hacl1/2 DKO +EtOH
Hacl1/2 DKO +2-OH C16:0 FA
B
even-numbered PC
PC (pmol/μg protein)
5
4
3
2
1
0
C16:1/16:0
C16:0/16:0
C16:1/18:1
C16:0/18:1
C18:1/18:1
C18:1/18:0

Fig. S7

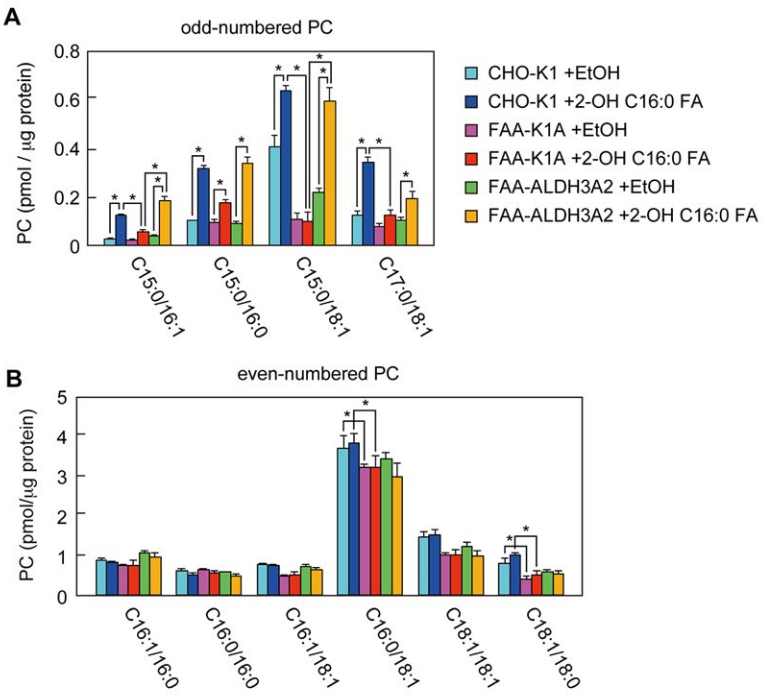
A
odd-numbered PC
PC (pmol / μg protein)
0.8
0.6
0.4
0.2
0
C15:0/16:1
C15:0/16:0
C15:0/18:1
C17:0/18:1
CHO-K1 +EtOH
CHO-K1 +2-OH C16:0 FA
FAA-K1A +EtOH
FAA-K1A +2-OH C16:0 FA
FAA-ALDH3A2 +EtOH
FAA-ALDH3A2 +2-OH C16:0 FA
B
even-numbered PC
PC (pmol/μg protein)
5
4
3
2
1
0
C16:1/16:0
C16:0/16:0
C16:1/18:1
C16:0/18:1
C18:1/18:1
C18:1/18:0